Title

Systematic Analyses of rpm-1 Suppressors Reveal Roles for ESS-2 in mRNA Splicing in Caenorhabditis elegans

Journal

Genetics, 198(3)

ISSN

0016-6731

Authors

Noma, Kentaro
Goncharov, Alexandr
Jin, Yishi

Publication Date

2014-11-01

DOI

10.1534/genetics.114.167841

Peer reviewed

Systematic Analyses of *rpm-1* Suppressors Reveal Roles for ESS-2 in mRNA Splicing in *Caenorhabditis elegans*

Kentaro Noma,*,† Alexandr Goncharov,*,† and Yishi Jin*,†,1

*Neurobiology Section, Division of Biological Sciences, and †Howard Hughes Medical Institute, University of California, San Diego, La Jolla, California 92093

ABSTRACT The PHR (Pam/Highwire/RPM-1) family of ubiquitin E3 ligases plays conserved roles in axon patterning and synaptic development. Genetic modifier analysis has greatly aided the discovery of the signal transduction cascades regulated by these proteins. In *Caenorhabditis elegans*, loss of function in *rpm-1* causes axon overgrowth and aberrant presynaptic morphology, yet the mutant animals exhibit little behavioral deficits. Strikingly, *rpm-1* mutations strongly synergize with loss of function in the presynaptic active zone assembly factors, *syd-1* and *syd-2*, resulting in severe locomotor deficits. Here, we provide ultrastructural evidence that double mutants, between *rpm-1* and *syd-1* or *syd-2*, dramatically impair synapse formation. Taking advantage of the synthetic locomotor defects to select for genetic suppressors, previous studies have identified the DLK-1 MAP kinase cascade negatively regulated by RPM-1. We now report a comprehensive analysis of a large number of suppressor mutations of this screen. Our results highlight the functional specificity of the DLK-1 cascade in synaptogenesis. We also identified two previously uncharacterized genes. One encodes a novel protein, SUPR-1, that acts cell autonomously to antagonize RPM-1. The other affects a conserved protein ESS-2, the homolog of human ES2 or DGCR14. Loss of function in *ess-2* suppresses *rpm-1* only in the presence of a *dlk-1* splice acceptor mutation. We show that ESS-2 acts to promote accurate mRNA splicing when the splice site is compromised. The human DGCR14/ES2 resides in a deleted chromosomal region implicated in DiGeorge syndrome, and its mutation has shown high probability as a risk factor for schizophrenia. Our findings provide the first functional evidence that this family of proteins regulate mRNA splicing in a context-specific manner.

PROPER synapse development ensures precise wiring and efficient transmission of information in the nervous system. In the presynaptic terminals, dense and organized accumulation of synaptic vesicles around the docking site called active zone is essential for rapid release of neurotransmitters (Sudhof 2012). Forward genetic screens in *Caenorhabditis elegans*, aided by visualization of synapse morphology using fluorescent reporters, have made important contributions to uncover conserved genes and pathways regulating presynaptic assembly (Jin and Garner 2008; Ou and Shen 2010). Many such screens have identified a common set of genes that regulate specific aspects of presynaptic differentiation in many neurons (Ackley and Jin 2004; Jin 2005; Maeder and Shen 2011). Among them are SYD-2/α-Liprin (LAR interacting protein), which has a central role in presynaptic active zone formation (Zhen and Jin 1999; Dai *et al.* 2006); SYD-1, a PDZ-RhoGAP protein that acts upstream of SYD-2 (Patel and Shen 2009; Hallam *et al.* 2002); and RPM-1, an E3 ubiquitin ligase that regulates synaptic organization (Schaefer *et al.* 2000; Zhen *et al.* 2000).

Despite their strong defects in synaptic morphology, single loss-of-function (*lf*) mutants of *rpm-1*, *syd-1*, or *syd-2* generally exhibit subtle to mild impairment in most behavioral assays. However, double mutants of *rpm-1(lf)* with *syd-1(lf)* or *syd-2(lf)* show more severe uncoordinated movement than expected from simple additivity of the single mutants (Liao *et al.* 2004; Nakata *et al.* 2005), indicating that *rpm-1* acts in parallel to *syd-1* and *syd-2*. This synthetic behavioral deficit of double mutants has allowed powerful selections for genetic suppressor mutations. Previous characterization of multiple *rpm-1(lf)* suppressors uncovered the DLK-1 MAP kinase pathway, consisting of *dlk-1*/MAPKKK, *mkk-4*/MAPKK, *pmk-3*/MAPK, and *mak-2*/MAPKAP2, *uev-3*/E2 ubiquitin-conjugating

doi: 10.1534/genetics.114.167841
Manuscript received July 8, 2014; accepted for publication August 28, 2014; published Early Online September 5, 2014.
Supporting information is available online at http://www.genetics.org/lookup/suppl/doi:10.1534/genetics.114.167841/-/DC1.
[1]Corresponding author: 9500 Gilman Drive, La Jolla, CA 92093-0368. E-mail: yijin@ucsd.edu

enzyme variant, and *cebp-1*, a bZip-domain transcription factor acting downstream of the DLK-1 kinase cascade (Nakata *et al.* 2005; Yan *et al.* 2009; Trujillo *et al.* 2010). Further analysis of specific DLK-1 missense alterations also provided key insights into the mechanism of DLK-1 activation (Yan and Jin 2012). In addition, the identification of a gain-of-function allele of *syd-2* as a suppressor of *syd-1* revealed the order of activity in presynaptic active zone assembly (Dai *et al.* 2006).

To gain a more complete understanding of the genetic interaction landscape on the behavioral suppression of *rpm-1*; *syd-1* or *rpm-1*; *syd-2*, here, we have characterized 95 suppressors. We uncovered a new allele of the *sup-5* amber suppressor gene as the sole mutation suppressing *syd-2*. Of the 94 *rpm-1* suppressors, 92 affected previously known components of the DLK-1 cascade. Interestingly, although the MLK-1 kinase cascade acts in parallel to the DLK-1 pathway in axon regeneration (Nix *et al.* 2011), we did not identify any mutations in the MLK-1 cascade in our screen. We showed that the loss-of-function mutations in this pathway do not suppress *rpm-1* developmental defects. Of the two remaining *rpm*-1 suppressors, one defined a novel gene *supr-1*. The other suppressor resulted in a loss of function in the homolog of the human DGCR14 gene, *ess-2*. Our analysis of a synthetic interaction between *ess-2* and a splicing mutation of *dlk-1* provides the first evidence that *ess-2* is functionally important in mRNA splicing.

Materials and Methods

C. elegans genetics and strains

We maintained *C. elegans* strains on NGM plates as described (Brenner 1974). We used *juIs1[Punc-25-SNB-1::GFP]* (Hallam and Jin 1998) to visualize presynaptic terminals of GABAergic motor neurons, *muIs32[Pmec-7-GFP]* (Ch'ng *et al.* 2003) for axonal morphology of mechanosensory neurons. All strains were maintained at 22.5°. Mutations and integrated lines were generally outcrossed to N2 more than four times before analyses. Strains and their genotypes are summarized in Supporting Information, Table S2.

Suppressor screen, genetic mapping, and whole-genome sequencing

Screens for suppressors of *syd-1(lf)*; *juIs1*; *rpm-1(lf)* or *juIs1*; *rpm-1(lf)*; *syd-2(lf)* were carried out using ethyl methanesulfonate (EMS) mutagenesis following standard procedures as described (Brenner 1974; Nakata *et al.* 2005). These double-mutant animals had minimal voluntary movements and could not move continuously even upon physical stimulation such as tapping. Suppressed worms showed continuous sinusoidal movements although they were slower than wild type (Figure S2). We first sorted new suppressors into complementation groups by testing known loci, following the scheme shown in Figure S1. We then determined the molecular lesions in these mutations by Sanger sequencing. The remaining candidates were either sequenced for the coding sequences of *mak-2*, *uev-3*, and *cebp-1* or subjected to whole-genome sequencing (WGS). In brief, genomic DNA was prepared from three 15-cm plates for each strain using Puregene Cell and Tissue kit (Qiagen, Valencia, CA) according to the manufacturer's instructions. Purified genomic DNAs were analyzed at Beijing Genomics Institute (BGI Americas). The obtained raw sequences were compared to the reference sequences in the WormBase using MAQGene software (Bigelow *et al.* 2009). By subtracting common variants among the cohort of suppressor strains, we determined unique homozygous single nucleotide polymorphism (SNP) variants for each strain. We then outcrossed each suppressor strain to N2 and performed further linkage analysis on the isolated recombinants based on the phenotypic suppression using the unique SNPs. *ju1041* was mapped to the middle of chromosome III, in a region containing the mutation in *sup-5* gene. *ju1118* was mapped to the middle of chromosome I, and only *supr-1* had a premature stop codon in this region. The suppression in CZ5301 *dlk-1(ju600)I*; *syd-1(ju82)II*; *ess-2(ju1117)III*; *juIs1IV*; *rpm-1(ju44)V* showed linkage to two regions, the right arm of chromosome I and the middle of chromosome III. We found a splice mutation in *dlk-1* on chromosome I. Complementation test of *dlk-1(ju600)* to *dlk-1(0)* showed that *dlk-1(ju600) per se* has no noticeable suppression on behavioral phenotypes of *syd-1(lf)*; *rpm-1(lf)*. We then found a premature stop codon mutation in the *ess-2* gene on chromosome III to be necessary for the suppression of *rpm-1(lf)*.

Behavioral analysis using a multiworm tracker

Locomotion speed was recorded using an automated multiworm tracking system as previously described (Pokala *et al.* 2014). Briefly, to restrict animal movement to the tracking area, filter paper with a 1-square-inch hole was soaked with 100 mM $CuCl_2$ solution and placed onto a food-free agar plate. Ten young adult worms were transferred to a food-free assay plate after briefly washing in M9 solution, and allowed to crawl for 20 min before recording. Video recordings were acquired at 3 Hz using Streampix software (Norpix, Quebec, Canada) and a PL B-741F camera (PixeLINK, Ontario, Canada) with a Zoom 7000 lens (Navitar, Rochester, NY), and were analyzed with custom software written in MATLAB (Mathworks). The average velocity of forward locomotion was obtained from 5–10 worms for each session, and three sessions were averaged to obtain the average speed for each genotype.

DNA constructs

cDNAs were amplified from an N2 cDNA library using gene-specific primers shown below. The cDNAs were cloned into pCR8 or pDONR221 vector to make entry clones compatible with the Gateway system (Invitrogen, Carlsbad, CA), and the DNA sequences were confirmed by Sanger sequencing. Wild-type (wt) *ess-2* cDNA (F42H10.7b in WormBase, 1596 bp including ATG to the stop codon; see Figure 5A) was cloned using the primers YJ9222: 5′-ATGtcgtcgttcgacaaaaat-3′ and YJ9172: 5′-TTAgaaaaagtctccagcatt-3′ (pCZGY2377).

ess-2(ju1117) and *ess-2(ok3569)* cDNAs (pCZGY2552 and pCZGY2553) were cloned from the cDNA libraries obtained from each mutant strain. These entry vectors were recombined with *Pmec-4*-GTW (pCZGY553) to make *Pmec-4*–ESS-2 (wt, pCZGY2379; ju1117, pCZGY2554; ok3569, pCZGY2555) for the rescue experiments. pCZGY2377 was recombined with *Pmec-4*–GFP–GTW (pCZGY603) to generate *Pmec-4*–GFP::ESS-2 (pCZGY2381). To construct GFP-tagged ESS-2, *ess-2* cDNA (1587 bp without stop codon) was cloned using the primers (YJ9222 and YJ10311: 5′-gaaaaagtctccagcatttgc-3′). This entry clone (pCZGY2378) was recombined with *Pmec-4*–GTW–GFP (pCZGY858) to make *Pmec-4*–ESS-2::GFP (pCZGY2380). *supr-1* cDNA (Y71F9AR.3 in WormBase, 2241 bp including ATG to the stop codon) was cloned using the primers YJ10312: 5′-ATGaagctagaggattcttgtgcc-3′ and YJ10313: 5′-TCAatgttctaaatttttcgaaacaat-3′. This entry clone (pCZGY2382) was recombined with pCZGY553 or pCZGY603 to generate *Pmec-4*–SUPR-1 (pCZGY2383) or *Pmec-4*–GFP::SUPR-1 (pCZGY2384). A short isoform of *supr-1* lacking exon 4 (see Figure 3A) was identified, but not used in this study. *rpm-1* cDNA (C01B7.6 in WormBase) was cloned into pDONR221 vector as three restriction enzyme-digested fragments ligated into one piece (pCZGY2005). GFP was inserted into the *Pst*I site (pCZGY2017). This entry vector was recombined with *Prgef-1*–GTW (pCZGY66) to make *Prgef-1*–RPM-1::GFP (pCZGY2551).

Generation of transgenic C. elegans

Multicopy transgenic animals were generated as described (Mello *et al.* 1991). *Pttx-3*–RFP was used as a coinjection marker to adjust the total amount of DNA to 100 ng/μl. To rescue *ess-2*, we amplified the genomic fragment from N2 lysis using YJ10528: 5′-ccggccaaaggaacatccgaac-3′ and YJ10529: 5′-aagtggataaaggtccggcaaga-3′, and the DNA products were purified and injected into CZ17517 *dlk-1(ju600)*; *muIs32*; *ess-2(tm4246)*; *rpm-1(ju44)* at 1 ng/μl. pCZGY2379, pCZGY2554, or pCZGY2555 at 10 ng/μl was injected into CZ17517. pCZGY2383 at 10 ng/μl was injected into CZ17724 *supr-1(ju1118)*; *muIs32*; *rpm-1(ju44)* animals. For GFP-tagged ESS-2 and SURP-1 the following constructs were injected to test their rescue activities: pCZGY2380 or pCZGY2381 at 90 ng/μl was injected into CZ17517. pCZGY2384 at 10 ng/μl was injected into CZ17724. These strains were outcrossed to N2 to get rid of all the background mutations to observe GFP signals. In general, more than three lines were analyzed for each construct, and quantification data of one representative line was shown. For RPM-1::GFP transgene (*juEx3996*), pCZGY2383 at 50 ng/μl was injected into CZ1234 *rpm-1(ju23)* animals. This extrachromosomal array (*juEx3996*) was integrated into a chromosome to generate *juIs390* following ultraviolet trimethylpsoralen (UV/TMP) mutagenesis.

RNA preparation, RT-PCR, and qRT-PCR

Young adult worms were collected from three 60-mm NGM plates. Total RNA was extracted from whole animals using TRIzol reagent (Invitrogen) and treated with DNase I (Roche, Indianapolis, IN) for 20 min at 37°. Two micrograms of total RNA were reverse transcribed into cDNA using random primers and the SuperScript III First-Strand Synthesis system (Invitrogen) following the manufacturer's instructions. For semiquantitative RT-PCR, cDNA fragments were amplified using the primers: *dlk-1* pair flanking *ju600* mutation site (YJ10323: 5′-gtcgaaacccagcctgaac-3′ and YJ10324: 5′-ctcggtctccttcagttg-3′; see Figure 6A), *dpy-1* pair flanking *e128* mutation site (D1: 5′-cacattttcaagtgaagacttgag-3′ and D2: 5′-ggtcctggaatgcaacatcct-3′) (Aroian *et al.* 1993), and *ama-1* pair (YJ2492: 5′-gcattgtctcacgcgttcag-3′ and YJ2493: 5′-ttcttccttctccgctgctc-3′) as a control and analyzed by agarose gel electrophoresis. For quantitative RT-PCR Power SYBR Green PCR Master Mix (Applied Biosystems, Foster City, CA) the kit was used for the reactions and the products were detected in real time using the ABI Prism 7000 Sequence Detection system. cDNAs were amplified using the following primer pairs in which forward or reverse primers were designed to anneal the exon–exon junction to avoid amplification from genomic DNA (see Figure 6A): *dlk-1* exon 3–4 pairs (YJ10317: 5′-gggctcttttcgtgttttcagc-3′ and YJ10318: 5′-cctcggatttttcaatttcaactg-3′), *dlk-1* exon 5–6 pairs (YJ10319: 5′-tgttggaacaaacattctgagcc-3′ and YJ10320: 5′-ggagaatgagggacgattgcg-3′), *dlk-1* exon 8–9 pairs (YJ10321: 5′-gcgaatccgccaaaaatcctac-3′ and YJ10322: 5′-cggaatccctg gccggtgat-3′), and ribosomal subunit S25 (*rps-25*) pairs as an internal control (*rps-25* F: 5′-ctctacaaggaggtcatcacc-3′ and *rps-25* R: 5′-gacctgtccgtgatgatgaacg-3′). The *dlk-1* mRNA levels were normalized to *rps-25* for each product and then normalized to the control strain.

Bright-field and fluorescence microscopy

Bright-field images were photographed using a Leica MZ95 stereomicroscope (Leica Microsystems, Buffalo Grove, IL). For quantification of the morphology of mechanosensory neurons using *muIs32[Pmec-7-GFP]* reporter, young adults were immobilized in 1% phenoxypropanol (TCI America, Portland, OR) in M9 buffer and scored under a Zeiss Axioplan 2 microscope equipped with Chroma HQ filters and a ×63 (NA = 1.4) objective lens. Images of the fluorescent reporters were collected from young adults immobilized in M9 with 1% phenoxypropanol using a Zeiss LSM710 confocal microscope equipped with ×63 (NA = 1.4) or ×100 (NA = 1.46) objective lens. Images shown are maximum-intensity projections obtained from several *z*-sections (0.5–1.0 μm/section).

Electron microscopy

CZ333 *juIs1*, CZ840 *juIs1*; *rpm-1(ju41)*; *syd-2(ju37)*, and CZ1797 *syd-1(ju82)*; *juIs1*; *rpm-1(ju44)* young adult animals were fixed using glutaraldehyde and osmium as described (Hallam *et al.* 2002). Midanterior body was serially sectioned at 40–50 nm thickness. The ventral and dorsal nerve cords were photographed using a JEOL 1200EX transmission electron microscope (JEOL, Tokyo, Japan) at 80 kV. Presynaptic terminals of neuromuscular junctions were defined by the existence of clear synaptic vesicles and electron-dense active zones. The types of the motor neurons, cholinergic or

GABAergic, were defined by the synaptic connections (White *et al.* 1986). Synaptic vesicles were morphologically determined as 35–50 nm clear vesicles, and their numbers were manually counted in the sections containing the active zone.

Statistical analysis

We analyzed the *rpm-1(lf)* phenotypes of the mechanosensory neurons using Fisher's exact test in GraphPad Prism 5.0 (GraphPad Software, La Jolla, CA). Locomotion speed and synaptic vesicle numbers were analyzed using one-way ANOVA and Bonferroni's multiple comparison test in GraphPad Prism 5.0.

Results

Presynaptic development is severely disrupted in double mutants of rpm-1 with syd-1 or syd-2

We previously reported that null (0) mutations of *rpm-1* result in disorganized synapses (Zhen *et al.* 2000), and null mutations of *syd-1* or *syd-2* alter presynaptic active zone assembly (Zhen and Jin 1999; Hallam *et al.* 2002). By gross movement, *rpm-1(0)* is indistinguishable from wild type, and *syd-1(0)* and *syd-2(0)* show slow movement while maintaining sinusoidal pattern (Figure 1, A and B). Strikingly, *rpm-1*; *syd-1* and *rpm-1*; *syd-2* double mutants show severely uncoordinated behavior from young larvae throughout mature adults (Figure 1B). Their body size and brood size are also smaller than wild-type animals or each single mutant (Figure 1A, and data not shown). We quantified locomotion behavior using a multi-worm tracker. Wild-type worms showed a coordinated sinusoidal movement, with an average forward locomotion speed of 167.1 ± 15.6 μm/sec. While movement speed for each single mutant was similar to that of wild type, the *rpm-1*; *syd-2* double mutants greatly reduced the speed to 18.2 ± 0.7 μm/sec (mean ± SEM, $n = 3$ experiments, 5–10 worms/experiment) (Figure 1, A and B). Panneuronal expression of *rpm-1*(+) using a transgene *juIs390[Prgef-1-RPM-1::GFP]* rescued both the uncoordinated behavior and small body size of *rpm-1*; *syd-2* double mutants (Figure 1, A and B), suggesting that the behavioral and body size defects arise from the loss of *rpm-1* function in neurons and that the body size may be a secondary effect associated with severe paralysis.

The behavioral deficits of these double mutants are strongly correlated with severe disruption of synapses in many neurons. The motor neurons form *en passant* synapses onto ventral and dorsal body wall muscles (White *et al.* 1986). A synaptic vesicle marker such as *juIs1[Punc-25-SNB-1::GFP]* readily enables visualization of the presynaptic terminals of GABAergic motor neurons (Figure 1C) (Hallam and Jin 1998). *rpm-1*, *syd-1*, and *syd-2* single mutant animals each display distinctive alterations in presynaptic morphology, as previously described (Figure 1C) (Zhen and Jin 1999; Zhen *et al.* 2000; Hallam *et al.* 2002). In *rpm-1*; *syd-1* or *rpm-1*; *syd-2* double mutants, SNB-1::GFP puncta were barely detectable in the presumed presynaptic regions along the nerve processes (Figure 1C). Examination of several synaptic markers in other types of neurons revealed similar reduction in synapse number and abnormal synapse morphology (data not shown). The morphological defects of presynaptic terminals were observed from young larvae through adults, consistent with the behavioral deficit throughout development.

We further examined the presynaptic architecture of motor neurons using electron microscopy on serial ultrathin sections. Presynaptic terminals of these neurons are identified as axonal swellings containing clusters of synaptic vesicles and electron dense active zones (Figure 1D) (White *et al.* 1986). We analyzed segments of ventral and dorsal nerve cords (~250 sections, corresponding to ~11.25 μm) in two mutant strains (*syd-1*; *juIs1*; *rpm-1* and *juIs1*; *rpm-1*; *syd-2*) and *juIs1* as a control. Both double mutants displayed dramatically reduced numbers of synapses in cholinergic and GABAergic motor neurons (Table 1 and Figure 1, E and F). Furthermore, the few remaining synapses contained very few synaptic vesicles that were scattered near the presynaptic dense projections (Figure 1, D–F), indicating that presynaptic terminals were poorly developed and/or maintained in the double mutants. These analyses show that the *rpm-1* pathway and the presynaptic active zone assembly pathway via *syd-1/syd-2* function in parallel to promote presynaptic development.

Most suppressors of the developmental defects of rpm-1 affect the DLK-1 kinase cascade

We exploited the synthetic locomotor deficits of *rpm-1*; *syd-1* and *rpm-1*; *syd-2* double mutants to select for mutations that improved movement (see *Materials and Methods*). Subsequent analyses of the GABAergic presynaptic morphology using the *Punc-25-SNB-1::GFP* marker allowed us to sort the suppressor mutations into groups that displayed specific suppression on each gene. Although the screen should have an equal chance to isolate mutations suppressing either gene, of the 95 suppressors analyzed, we found only one allele, *ju1041*, that specifically suppressed *syd-2(ju37)*, but not *rpm-1(lf)* (data not shown). *syd-2(ju37)* results in an amber stop codon at Glu397 (Zhen and Jin 1999). We mapped *ju1041* to the middle of chromosome III (Figure 2C) and identified a single nucleotide change from C to T in *sup-5*, a tryptophan tRNA (see *Materials and Methods*). The mutated tRNA in *ju1041* can encode tryptophan for the amber stop codon as previously described (Waterston and Brenner 1978; Wills *et al.* 1983). The isolation of *sup-5(ju1041)* as the only suppressor of *syd-2(ju37)* suggests that few genes can be mutated to bypass the requirement for *syd-2(lf)* in synapse development and function.

The remaining 94 suppressors we characterized were specific for *rpm-1*. We previously reported multiple *rpm-1* suppressors that cause loss of function in components of the DLK-1/MKK-4/PMK-3 MAP kinase pathway (Figure 2A and Figure S2) (Nakata *et al.* 2005; Yan *et al.* 2009; Trujillo *et al.* 2010). We therefore devised a complementation workflow to test whether new suppressors affected these known genes

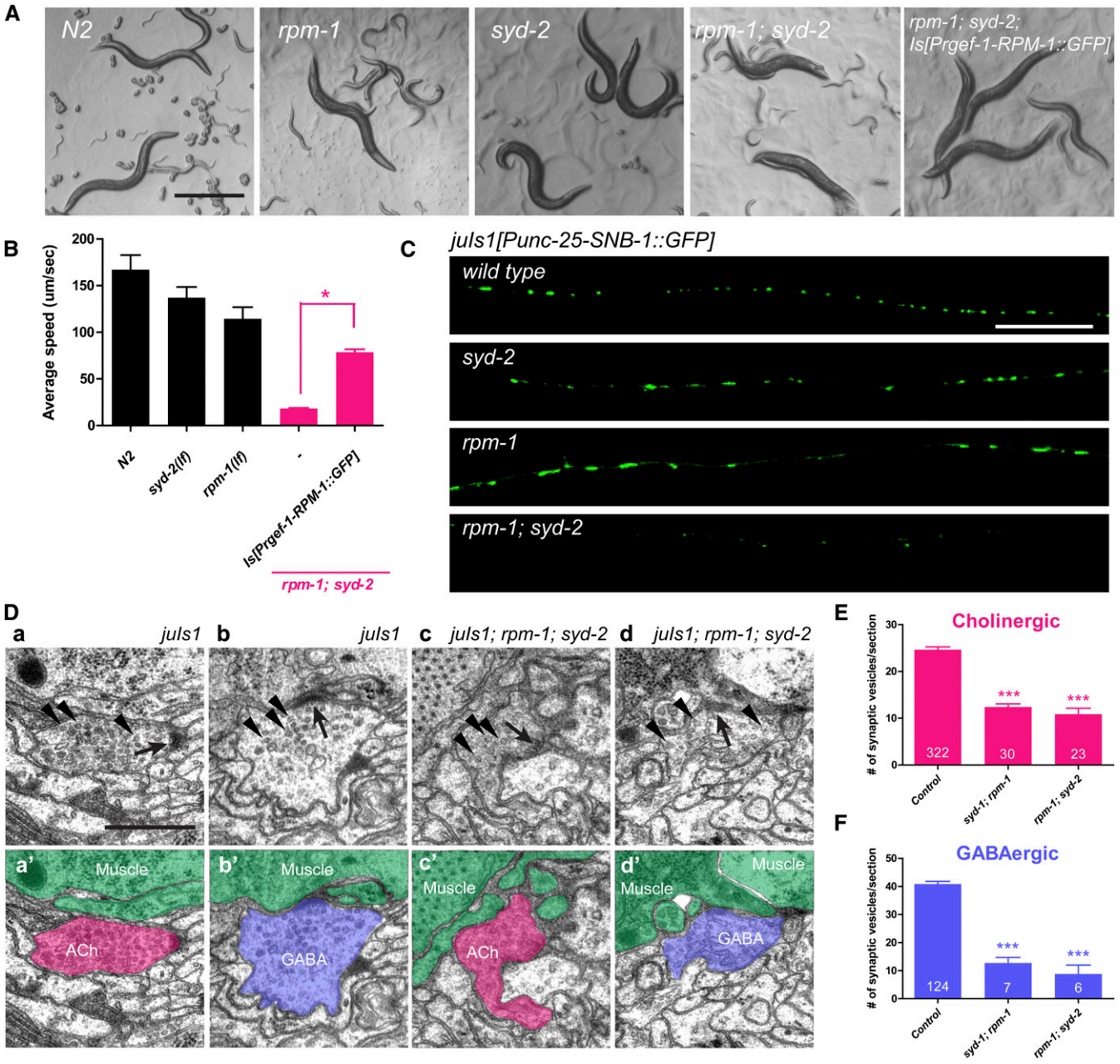

Figure 1 *rpm-1(lf)* synergizes with *syd-1(lf)* and *syd-2(lf)* to impair locomotion and presynaptic morphologies. (A) Bright-field images showing the body shapes of adult animals for the indicated genotypes. Bar, 500 μm. (B) Locomotion speed of worms for the indicated genotypes was analyzed using a multiworm tracker. Average velocity of the forward movement was calculated for 15-min sessions. Error bar indicates SEM. Statistics: one-way ANOVA, $*P < 0.05$. (C) Presynaptic terminals in the dorsal cord visualized by *juls1[Punc-25-SNB-1*::*GFP]*, genotype of animals indicated. In *rpm-1(lf)* mutant, the numbers of presynaptic terminals are decreased and remaining synapses either overdeveloped or immature (Zhen *et al.* 2000). *syd-2(lf)* mutants have comparable number of synapses but the synaptic vesicles show diffused pattern (Zhen and Jin 1999). Hardly any SNB-1::GFP was observed in *rpm-1(lf)*; *syd-2(lf)*. Bar, 20 μm. (D) Electron micrographs of presynaptic terminals. Arrowheads and arrows in a–d indicate synaptic vesicles and active zones, respectively. In a'–d' presynaptic varicosities of cholinergic and GABAergic neurons are shown in magenta and blue, respectively. Muscles are shown in green. AZ, active zone. Bar, 500 nm. (E and F) Average number of synaptic vesicles in sections containing active zones was analyzed for cholinergic neurons (E) and GABAergic neurons (F). *n* = no. of sections. Error bar indicates SEM. Statistics: one-way ANOVA, compared with control. $***P < 0.001$. Alleles and transgene used: rpm-1(ju23), rpm-1(ju44), rpm-1(ju41), syd-1(ju82), syd-2(ju37), and juls390[Prgef-1-RPM-1::GFP].

(Figure S1 and *Materials and Methods*). Among 94 suppressors, 41 were determined to be alleles of *dlk-1* and 26 were alleles of *pmk-3* (Figure 2B and Table S1). Among the new suppressors that were not *dlk-1* or *pmk-3*, some were linked to *syd-2* on the X chromosome, where *mkk-4* and *cebp-1* reside (Figure 2C and Figure S2). Subsequent DNA sequencing analysis of candidate genes, in conjunction with whole-genome sequencing of selected suppressors, revealed single

Table 1 Severe reduction of synapse number and synaptic vesicles in *rpm-1; syd-1* or *rpm-1; syd-2* mutants

Genotype	Nerve cord	Type	No. of synapses/10 μm worm1	No. of synapses/10 μm worm2	Average length of synapses, μm
juls1	VC	ACh	8.7	4.4	0.58 ± 0.03 (n = 49)
		GABA	4.2	1.8	0.86 ± 0.05 (n = 23)
	DC	ACh	5.1	4.9	0.66 ± 0.05 (n = 34)
		GABA	2.4	1.8	1.01 ± 0.07 (n = 15)
juls1; rpm-1(ju41); syd-2(ju37)	VC	ACh	1.8	3.6	0.47 ± 0.06 (n = 6)
		GABA	0.9	0.9	0.50 ± 0.09 (n = 2)
	DC	ACh	0.9	0.9	0.47 ± 0.11 (n = 2)
		GABA	0.0	0.9	0.36 (n = 1)
syd-1(ju82); juls1; rpm-1(ju44)	VC	ACh	0.0	4.4	0.68 ± 0.10 (n = 5)
		GABA	0.0	0.9	0.54 (n = 1)
	DC	ACh	0.0	6.2	0.43 ± 0.06 (n = 7)
		GABA	0.9	1.8	0.56 ± 0.11 (n = 3)

Young adult worms were chemically fixed, processed, and serially sectioned. The ventral and dorsal cords of two worms per genotype were examined by electron microscope. Numbers of sections analyzed were ~1000 for *juls1* worm 1 (45 μm), ~500 for *juls1* worm 2 (22.5 μm), and ~250 for the others (11.25 μm). The synapses were defined as a varicosity containing synaptic vesicles and one or a few active zones (White *et al.* 1986). Synaptic vesicles were counted in the sections containing an active zone and averaged over sections. The length of a synapse was calculated by multiplying the number of sections containing synaptic vesicles by 50 nm. n = no. of synapses.

nucleotide changes in all six genes of the DLK-1 pathway, as summarized in Table S1 and Figure 2B. Most of the nucleotide changes in *dlk-1*, *mkk-4*, or *pmk-3* are predicted to cause missense alterations in the kinase domains (Yan and Jin 2012) (Figure 2D, Figure S3, and Figure S4). Seven *dlk-1* alleles, two *pmk-3* alleles, and one *mak-2* allele were independent isolates of the same nucleotide changes from different mutagenized parents, suggesting that the mutagenesis hits are likely saturated in the context of this screen for the behavioral suppression (Table S1). Among the collection of new alleles, we found several mutations that revealed potential roles of new functional domains. For example, two new alleles of *pmk-3*, *ju1010* and *ju592*, are nonsense mutations after the kinase domain, suggesting that the C terminus of PMK-3 may regulate the protein activity or stability. *cebp-1*(*ju634*) altered arginine 63 to proline in the N terminus of the protein, whereas the majority of the previously reported *cebp-1* mutations affect the bZip domain (Yan *et al.* 2009; Bounoutas *et al.* 2011) (Figure 2D and Table S1). In summary, 98% of the suppressor mutations identified in our screens affected the six genes of the DLK-1 kinase cascade (Figure 2A and Table S1), and the number of the identified alleles roughly correlated with the size of the coding regions of the genes (Figure 2B).

The MLK-1 kinase cascade has a minor role in the developmental phenotypes of rpm-1 mutants

Among other MAP kinase cascades in *C. elegans* (Sakaguchi *et al.* 2004), the MLK-1/MEK-1/KGB-1 pathway, has recently been shown to act in parallel to the DLK-1/MKK-4/PMK-3 pathway in axon regeneration (Nix *et al.* 2011). MLK-1::GFP expression levels are increased in *rpm-1* mutants, suggesting MLK-1, like DLK-1, may be a substrate for degradation by RPM-1. The *mlk-1*, *mek-1*, and *kgb-1* genes are comparable in size to the genes of the *dlk-1* pathway (Figure 2B), and null mutants in these genes are viable and behaviorally normal. However, we found none of the suppressor mutations isolated in our screen affected the genes in the MLK-1 pathway (Table S1). We therefore constructed a strain of *kgb-1(0)*; *rpm-1(lf)*; *syd-2(lf)*, and found no improvement on locomotor phenotype (Figure 3A). Previous studies showed that *mlk-1(0)* and *mek-1(0)* did not suppress the presynaptic defects in GABAergic neurons of *rpm-1(lf)* (Nakata *et al.* 2005). Here, to further assess the activity of *the mlk-1/mek-1/kgb-1* in neuronal development, we analyzed the axonal development of mechanosensory neurons. In *rpm-1(lf)* mutants the Posterior Lateral Microtubule (PLM) neurons display highly penetrant axon overshooting and frequent absence of synaptic branches (Schaefer *et al.* 2000) (Figure 3, B–D). These PLM axon developmental defects of *rpm-1(lf)* are completely suppressed by loss-of-function mutations in the DLK-1 cascade (Yan *et al.* 2009; Trujillo *et al.* 2010) (Figure 3, C and D). In contrast, null mutations in *mlk-1*, *mek-1*, or *kgb-1* showed rather mild suppression (Figure 3, C and D). *kgb-2* is a closely related homolog of *kgb-1*, sharing 84% identity. We found that the *kgb-1(0) kgb-2(0)* double mutant also did not strongly suppress *rpm-1(lf)* PLM axonal defects (Figure 3D). This additional analysis demonstrates the highly specific regulation of the DLK-1/MKK-4/PMK-3 cascade by RPM-1 in synapse and axon development.

Loss of function in a novel protein SUPR-1 suppresses rpm-1(lf)

We mapped the *rpm-1* suppressor mutation *ju1118* to the middle of chromosome I, following whole-genome sequencing analysis (Figure 2C and *Materials and Methods*). We found a single nucleotide change, G875A, resulting in Trp292 to a stop codon mutation in the predicted geneY71-F9AR.3, hereby named *supr-1* (*suppressor of rpm-1*) (Figure 4A and Figure S5). *supr-1(ju1118)* was a weak suppressor by the criterion of locomotion behavior (data not shown). Quantification of the suppression of *rpm-1(lf)* on the PLM axon defects also showed that *supr-1(ju1118)* exhibited weaker suppression activity than those due to complete loss of function in the *dlk-1* cascade (Figure 4B). We verified the *supr-1* gene structure by RT-PCR and cDNA analysis. We

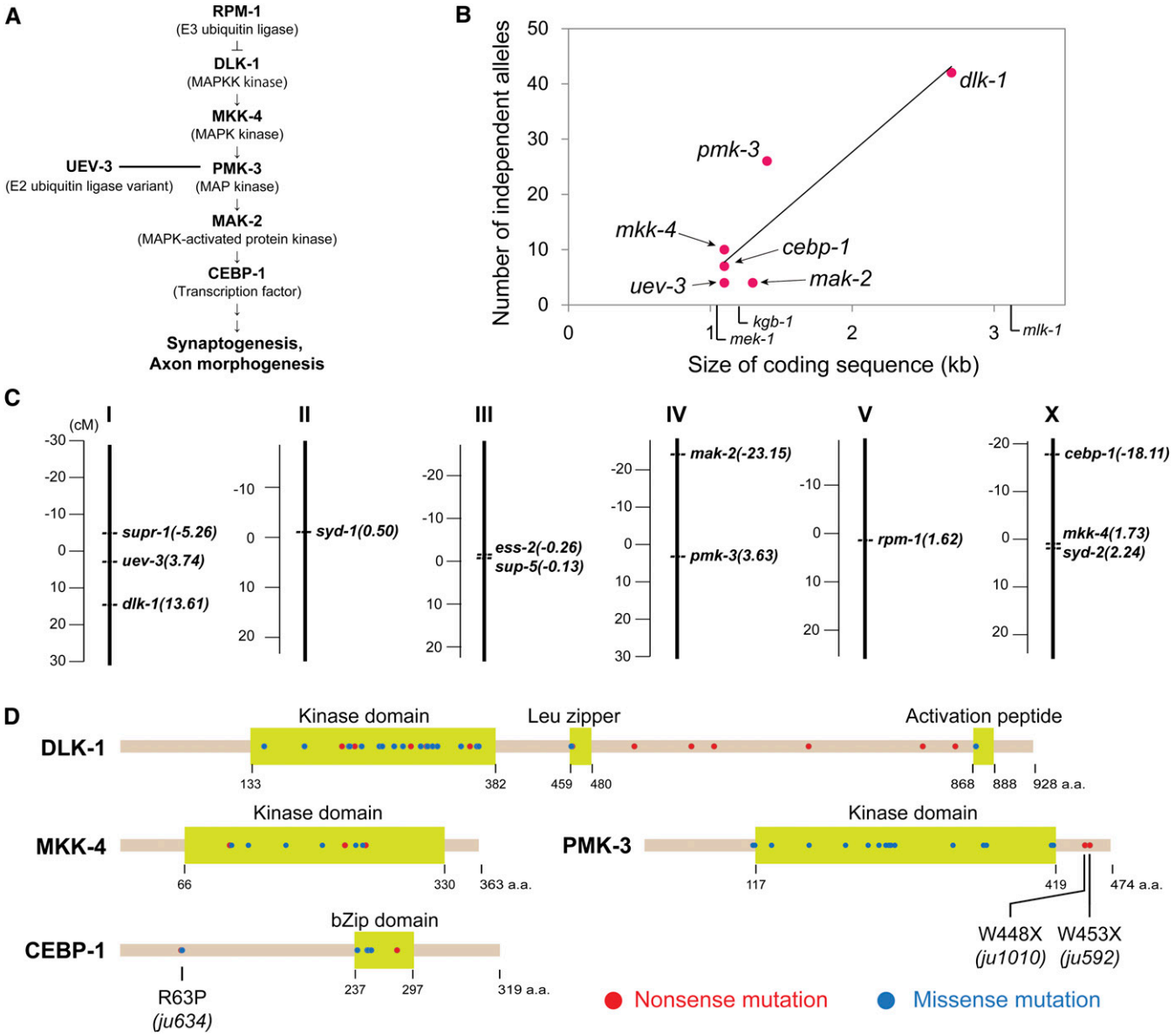

Figure 2 Most of the *rpm-1(lf)* suppressors are mutations in the core components of the DLK-1 cascade. (A) Schematic diagram of the known components of the DLK-1 pathway. E3 ubiquitin ligase RPM-1 down-regulates DLK-1 MAPKK kinase by degradation. (B) The total number of alleles for each gene in the DLK-1 cascade independently isolated in the suppressor screen was plotted against the length of the coding sequence. The method of "least squares" was used to obtain the linear approximation. The line represents $y = 22.1x - 16.6$. $R^2 = 0.81112$. The sizes of *mlk-1*, *mek-1*, and *kgb-1* are shown along the *x*-axis; no mutations were identified for these genes in our screen. (C) Genetic positions of the *rpm-1*, *syd-1*, *syd-2*, and their suppressor genes on the *C. elegans* chromosomes. Unit represents centimorgans (cM). (D) The positions of nonsense (red) and missense (blue) mutations isolated in the screen are plotted along the protein sequences. Functionally defined domains are shown as light green boxes. Positions of select alleles are indicated under the protein sequences (see *Results*).

identified two mRNA transcripts that differed in alternative exon 4, corresponding to two protein isoforms of 746 amino acids (long), and of 688 amino acids (short) (Figure 4A and Figure S5). To verify that *supr-1* is the causative gene for suppressing *rpm-1(lf)* phenotypes, we expressed the SUPR-1 long isoform cDNA under the mechanosensory neuron-specific promoter (*Pmec-4*). This transgene fully rescued the suppression phenotypes of *supr-1(ju1118)* (Figure 4C), confirming that *supr-1(ju1118)* is a loss of function mutation, and further, indicating that SUPR-1 functions cell autonomously.

The predicted SUPR-1 protein lacks known functional domains and has closely related proteins in other *Caenorhabditis* species (Figure S5). To gain insights into SUPR-1 function, we examined its localization in mechanosensory neurons using GFP-tagged SUPR-1 (long). This GFP-tagged construct fully rescued the *supr-1(ju1118)* effects on *rpm-1(lf)* (Figure 4C). GFP::SUPR-1 was primarily localized in the nucleus and weakly detectable in the somatic cytoplasm and axon (Figure 4D). We also analyzed two additional mutations of *supr-1*, *tm3467*, and *gk106345*. *tm3467* is a 327-bp

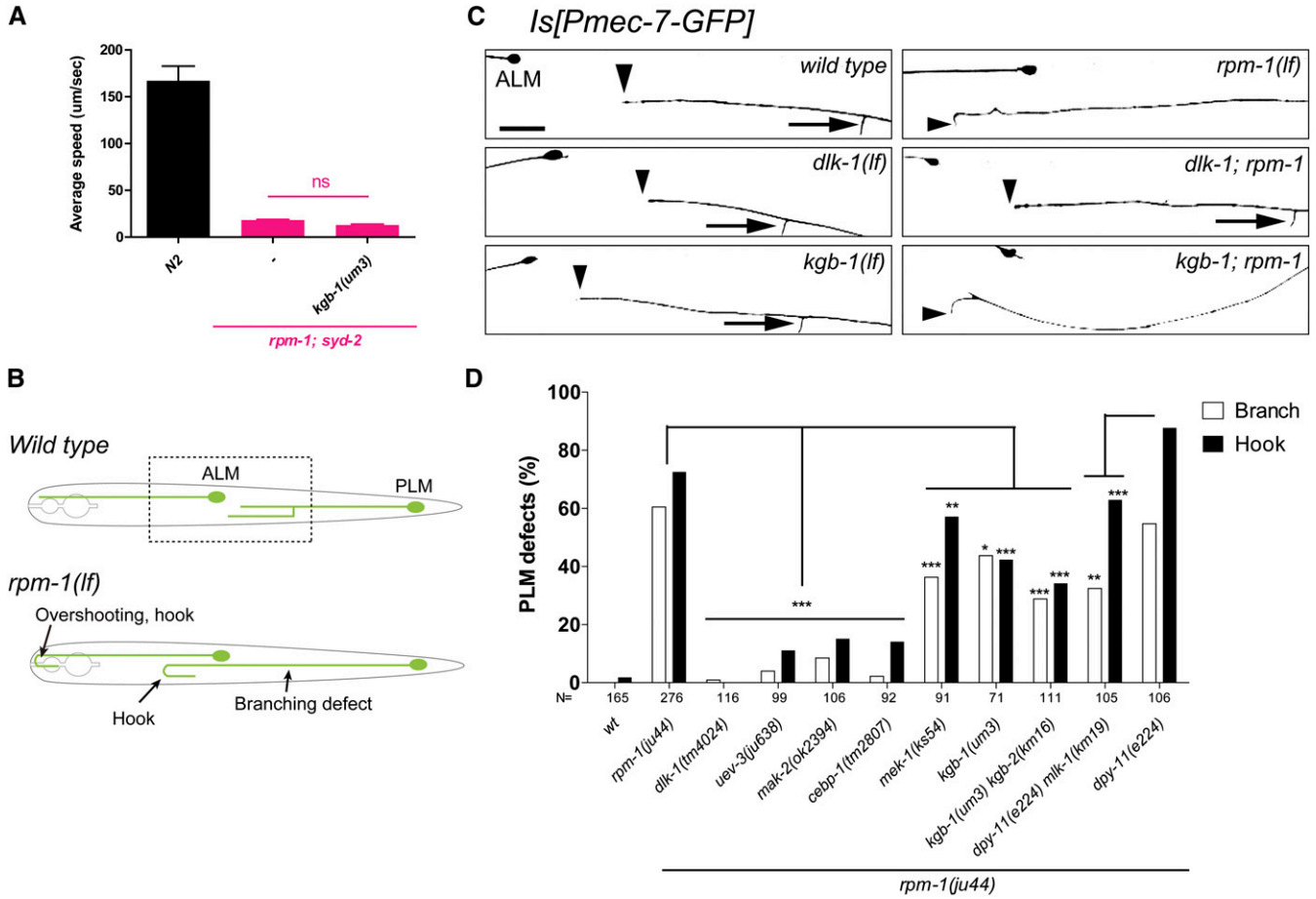

Figure 3 Loss of function in the core components of the MLK-1 cascade has modest effects on *rpm-1(lf)* developmental phenotypes. (A) The average velocities of the forward movement of the worms were analyzed as in Figure 1B. $n = 3$ sessions, 5–10 worms in each session. Error bar indicates SEM. Statistics: one-way ANOVA; ns, not significant ($P > 0.05$). (B) Schematic diagram of Anterior Lateral Microtubule (ALM) and PLM mechanosensory neurons shown in light green. In *rpm-1(lf)* mutants, ALM and PLM overshoot and hook back, and PLM shows no branch in ~50% of the animals (Schaefer *et al.* 2000). The micrographs of boxed region are shown in C. (C) The ALM and PLM were visualized by *muIs32[Pmec-7-GFP]* for the indicated genotypes. Arrows and arrowhead represent the axonal branch and tip of PLM neurons, respectively. Bar, 20 μm. (D) Fraction of worms showing PLM defects. Open bars and solid bars indicate branching and hook defects, respectively. *N* = no. of animals. *dpy-11(e224)* was used as a control for *dpy-11 (e224) mlk-1(km19)*. Statistics: Fisher's exact test, compared with *rpm-1(ju44)* to show suppression. $***P < 0.001$, $**P < 0.01$, $*P < 0.05$.

deletion removing the splice acceptor site of intron 7 and a part of exon 8. *gk106345* is a splice donor mutation in the exon 10/intron 10 junction (Figure 4A and Figure S5). mRNA may be produced from each allele using cryptic splice sites, but the encoded proteins would likely have an altered C-terminal region from Gly505 and Asn590 for *tm3467* and *gk106345*, respectively. We found that *tm3467* did not suppress the PLM morphological defects of *rpm-1(lf)*, while *gk106345* showed partial suppression, suggesting the SUPR-1 C terminus may likely be dispensible for its function (Figure 4B). Taken together, we identified a novel protein SUPR-1 that functions to antagonize *rpm-1*.

Loss of function in ess-2 synergizes with a splice acceptor mutation in dlk-1 to suppress rpm-1(lf)

In the course of analyzing a suppressor strain isolated from screening in the *rpm-1(ju44)*; *syd-1(ju82)* background, we identified the *ju600* allele as containing a single nucleotide change at the 3′ splice acceptor site (CAG to CAA) in the third intron of *dlk-1*. This change is predicted to result in the retention of intron 3 or skipping of exon 4, which would potentially lead to a premature stop codon before the kinase domain. However, we found that *dlk-1(ju600)* alone did not show detectable suppression on *rpm-1(lf)* (Figure 5D). By inspecting animals from outcrossing of the initial suppressor isolate, we detected a background-dependent suppression activity of *dlk-1(ju600)* that showed linkage to chromosome III. Through further genetic mapping using unique SNPs identified by whole-genome sequencing of the original suppressor strain, we identified a nonsense mutation in the *ess-2* (*ES2 similar*) gene (Dimitriadi *et al.* 2010) as required for *dlk-1(ju600)* to suppress *rpm-1(lf)* (Figure 5D). ESS-2 consists of 522 amino acids, and *ess-2(ju1117)* alters leucine 428 to a stop codon (Figure 5, A and B). The *ess-2(ju1117)* single mutation did not suppress *rpm-1(lf)*, but the *dlk-1(ju600)*; *ess-2(ju1117)* double mutant suppressed *rpm-1(lf)*, comparable

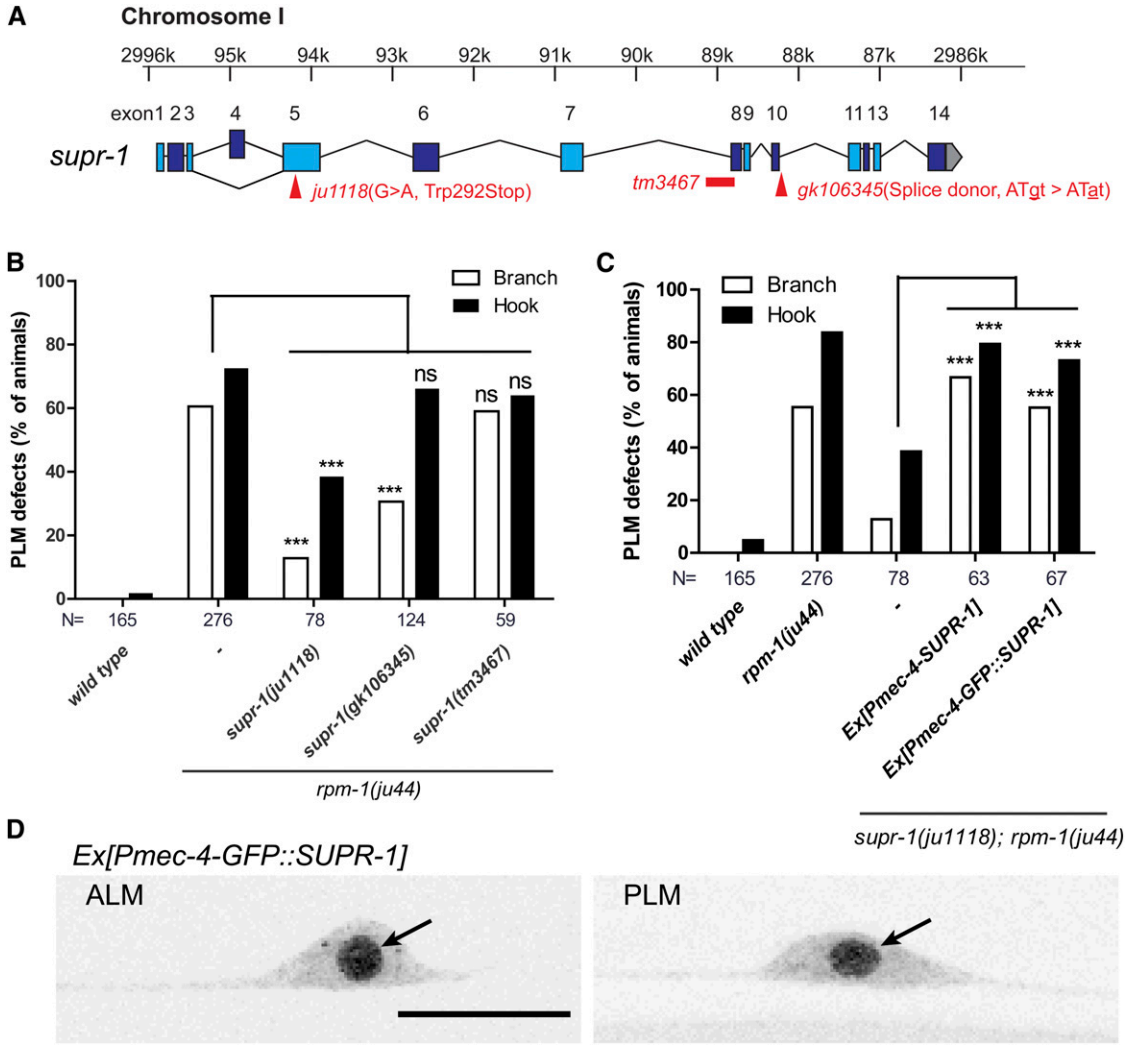

Figure 4 *supr-1* is a novel gene antagonizing *rpm-1*. (A) Schematic diagram of the genomic locus of *supr-1* (Y71F9AR.3 in WormBase). There are two isoforms produced from the locus as described in *Material and Methods*, but we focused on the long isoform in this study. (B and C) The fraction of worms showing defects of PLM axonal morphologies, as described in Figure 3, A and B. *N* = no. of animals. Statistics: Fisher's exact test, compared with *rpm-1(ju44)* to show suppression in B and with *supr-1(ju1118); rpm-1(ju44)* to show rescue activity in C. ***$P < 0.001$; ns, not significant ($P > 0.05$). (D) Localizations of SUPR-1 in the mechanosensory neurons were visualized by a transgene *juEx5517[Pmec-4-GFP::SUPR-1]*. Arrows indicate nucleus. Bar, 20 μm.

to the suppression by a *dlk-1* null allele (Figure 5D). We further analyzed two deletion alleles of *ess-2*, *tm4246*, and *ok3569* (Figure 5A and Figure S6). *tm4246* deletes a splice acceptor site of intron 1 through part of intron 4, and likely causes an early stop codon. *ok3569* removes parts of exon 3 and exon 4. We performed RT-PCR on *ok3569* animals and found that the remaining transcripts would result in an in-frame protein that lacks amino acids from Glu166 to Asp314 including a conserved coiled-coil domain (Figure 5B and Figure S6). Both *ess-2* alleles showed no suppression of *rpm-1(lf)* on their own and acted as synthetic suppressors with *dlk-1(ju600)* (Figure 5D). Furthermore, we generated transgenes expressing full-length *ess-2* genomic DNA, including 916 bp of the *ess-2* promoter region, and observed rescue of the synthetic suppression effects of *dlk-1(ju600); ess-2(tm4246)* (Figure 5E). These data demonstrate that *ess-2* is the causative gene for this synthetic suppression with *dlk-1(ju600)*. A transcriptional reporter driven by 916-bp upstream sequences of *ess-2* showed broad tissue expression, including neurons, pharynx, body wall muscles, and seam cells (data not shown). We thus generated transgenes expressing the *ess-2* cDNA under the control of mechanosensory neuron-specific promoter and found that this expression fully rescued the synthetic suppression effects on PLM in a cell-autonomous manner (Figure 5E). We infer that the *dlk-1(ju600)* splice site mutation is a cryptic *dlk-1* allele. Loss of function in *ess-2* enhances *ju600* to a complete loss of *dlk-1* function, resulting in the observed synthetic suppression of *rpm-1(lf)*.

ESS-2 is required for mRNA splicing of mutant dlk-1 (ju600) transcripts

C. elegans ESS-2 is named after the human protein ES2, also known as DiGeorge syndrome critical region 14 (DGCR14) or DiGeorge syndrome protein I (DGSI) (Lindsay *et al.* 1996;

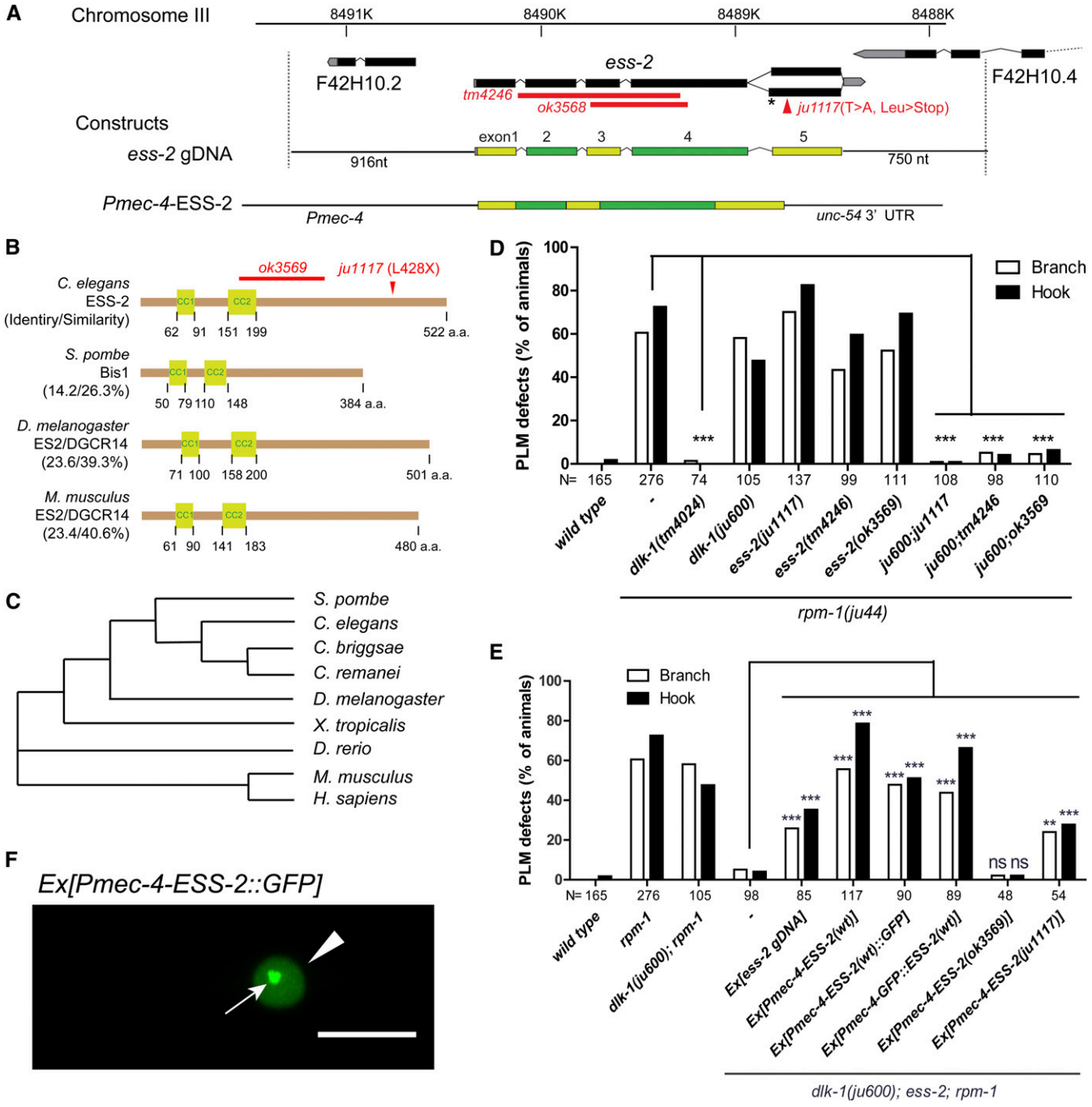

Figure 5 *dlk-1(ju600)* splice acceptor mutation suppresses *rpm-1(lf)* together with *ess-2(lf)*. (A) Schematic diagram of the genomic locus of *ess-2* and the DNA constructs for transgenes. The *ess-2* locus produces two isoforms, a and b (F42H10.7a and b in WormBase) that differ in six extra nucleotides at the beginning of exon 5 (asterisk). (B) Schematic diagrams of the domain structures of ESS-2 and its orthologs. Light green boxes indicate putative coiled-coil domains. (C) Dendrogram of the ESS-2 orthologs. The dendrogram was made using Clustal Omega. The names of ESS-2 homologs and accession nos. in UniProt are *S. pombe*: Bip1, O59793; *C. elegans*: ESS-2, P34420; *C. briggsae*: ESS-2, A8XT26; *C. remanei*: ESS-2, E3MI09; *Drosophila melanogaster*: ES2/DGCR14, O44424; *Xenopus tropicalis*, DGCR14, B1H164; *Danio rerio*: DGCR14, F1QAX0; *Mus musculus*: ES2/DGCR14/DGSI, O70279; and *Homo sapiens*: ES2/DGCR14/DGSI, Q96DF8. (D and E) The fraction of worms showing the defects of PLM axonal morphologies, as described in Figure 3, A and B. *N* = no. of animals. Statistics: Fisher's exact test, compared with *rpm-1(ju44)* to show suppression in D and with *dlk-1 (ju600)*; *ess-2(tm4246)*; *rpm-1(ju44)* to show rescue activity in E. ***$P < 0.001$; **$P < 0.01$; ns, not significant ($P > 0.05$). (F) Localization of ESS-2 in the PLM mechanosensory neuron was visualized by a transgene *juEx5859[Pmec-4-ESS-2::GFP]*. Arrowhead and arrow indicate nucleus and punctum, respectively. Bar, 20 μm.

Rizzu *et al.* 1996; Gong *et al.* 1997). This protein family is conserved from fission yeast *Schizosaccharomyces pombe* to human and contains two conserved coiled-coil regions in its N-terminal based on the MARCOIL program (Delorenzi and Speed 2002) (Figure 5B and Figure S6). Both yeast homolog Bis1 and mouse ES2 are localized in the nucleus (Lindsay *et al.* 1998; Taricani *et al.* 2002). A recent large-scale protein interactome study identified human ES2/DGCR14 as a non-core component of the spliceosome C complex (Hegele *et al.* 2012), suggesting that the ESS-2 protein family might function in mRNA splicing.

To investigate how ESS-2 functions, we next examined ESS-2 protein localization. We tagged ESS-2 with GFP at either the N or C terminus. Both constructs are fully functional based on transgenic rescue activity (Figure 5E). GFP-tagged ESS-2 was primarily localized to the nucleus, with occasional detection of one or a few bright nuclear puncta (Figure 5F). Similar nuclear puncta have also been reported for the fission yeast homolog, Bis1 (Taricani *et al.* 2002). Expression of cDNA isolated from *ess-2(ok3569)* did not rescue *ess-2(tm4246)*. Overexpression of cDNA containing *ess-2(ju1117)* mutation partially rescued *ess-2(tm4246)* (Figure 5E). This analysis suggests that the conserved coiled-coil domain is critical for ESS-2 function, and that C-terminally truncated ESS-2 protein produced in *ess-2(ju1117)* retains partial activity.

The observation that *dlk-1(ju600)* single mutants did not eliminate *dlk-1* activity suggests that this mutant likely produces sufficient functional DLK-1, despite the mutation altering the conserved splice acceptor consensus sequence. Early studies have indicated that the CAG in the splice acceptor site can be dispensable for mRNA splicing in *C. elegans* (Aroian *et al.* 1993). We thus examined the splicing of intron 3 of *dlk-1* by RT-PCR. Analysis of semiquantitative RT-PCR products showed that transcripts corresponding to the fully spliced transcripts were produced from *dlk-1(ju600)* animals to a comparable level of those from wild-type animals (Figure 6B). Sequence analysis also confirmed that mRNA splicing in *dlk-1(ju600)* used the same site as in *dlk-1(wt)* despite the nucleotide change at the splice acceptor site. On the other hand, transcripts corresponding to the unspliced transcript were only observed in *dlk-1(ju600)* (Figure 6B). In *ess-2(tm4246)* single mutants, we detected only fully spliced *dlk-1* transcripts, similar to wild-type animals (Figure 6B). However, in *dlk-1(ju600)*; *ess-2(tm4246)* double mutants the amount of fully spliced *dlk-1* transcripts was significantly decreased, compared to *dlk-1(ju600)* and wild type (Figure 6B). It is possible that RT-PCR may not detect transcript intermediates, such as those stalled in a Lariat structure (see *Discussion*). To more accurately assess the effects on mRNA splicing, we performed quantitative RT-PCR (qRT-PCR), using primers to specifically detect the transcripts in which intron 3 appeared to be spliced out (Figure 6A, magenta). Consistent with the semiquantitative RT-PCR data, we observed no detectable changes in either *dlk-1(ju600)* or *ess-2(ju1117)* single mutant, compared to wild type. However, spliced transcripts without intron 3 were dramatically decreased in *dlk-1(ju600)*; *ess-2(ju1117)* double mutant (Figure 6C, magenta). As a control for total mRNA level of *dlk-1*, we designed primers to detect exon 5–6 and exon 8–9 junctions (Figure 6A, gray and blue). qRT-PCR analysis showed that the amount of the *dlk-1* transcripts was not altered in *dlk-1(ju600)*; *ess-2(ju1117)* (Figure 6C, gray and blue), indicating that loss of function in *ess-2* specifically affects intron 3 splicing of *dlk-1*.

We next asked if ESS-2 has a similar role in splicing of other genes. The *dpy-10(e128)* mutation alters the splice acceptor from CAG to CAA in intron 1 of isoform "a" (Figure 6D). We performed RT-PCR for this exon/intron junction and detected both spliced and unspliced transcripts in *dpy-10(e128)*, consistent with a previous report (Aroian *et al.* 1993) (Figure 6E). In the *dpy-10(e128)*; *ess-2(tm4246)* double mutant, however, both spliced and unspliced bands were significantly reduced, suggesting that ESS-2 affects splicing efficiency of *dpy-10* transcripts when they carry the mutation in a splice acceptor site (Figure 6E). The effect of *ess-2(lf)* on the "a" isoform did not lead to further enhancement of dumpy body shape in *ess-2(lf)*; *dpy-10(e128)* compared to *dpy-10(e128)*, possibly because of residual activities of the "b" isoform (Figure 6D). Taken together, these data support a conclusion that ESS-2 acts to facilitate RNA splicing, particularly when pre-mRNA is compromised or contains non-canonical sequences at the splice acceptor site.

Discussion

Large-scale analysis of genetic suppressors of rpm-1 supports the functional specificity of the DLK-1 kinase cascade in synapse formation

Synapse formation is a terminal step in neuronal differentiation and involves coordinated action of multiple pathways, including recruitment and retention of synaptic vesicles, formation, and remodeling of synaptic cytoskeleton, assembly and alignment of junctional structures at pre- and postsynaptic sites. Genetic studies in *C. elegans* over the past decade have made important contributions to the delineation of key molecules and pathways in each specific aspect of synapse formation (Ackley and Jin 2004; Yan *et al.* 2011). Here, our analysis of *rpm-1*; *syd-1* and *rpm-1*; *syd-2* reinforces the notion that synaptogenesis is regulated by multiple parallel pathways. While removing each gene individually is not severely detrimental to animal behavior, these double mutants exhibit severely impaired movement, correlating to the dramatic reduction of synapse number and poorly developed remaining synapses. It is interesting to note that the locomotion defect of these double mutants is less severe than that of the kinesin *unc-104(lf)*, in which synaptic vesicles are nearly depleted while the localization of synaptic active zone proteins appears to be unperturbed (Hall and Hedgecock 1991; Zhen and Jin 1999). The behavioral outcome of *rpm-1(lf)*; *syd-2(lf)* might indicate that some residual neuronal activity remains in these animals due to compensation or use of different means of synaptic transmission.

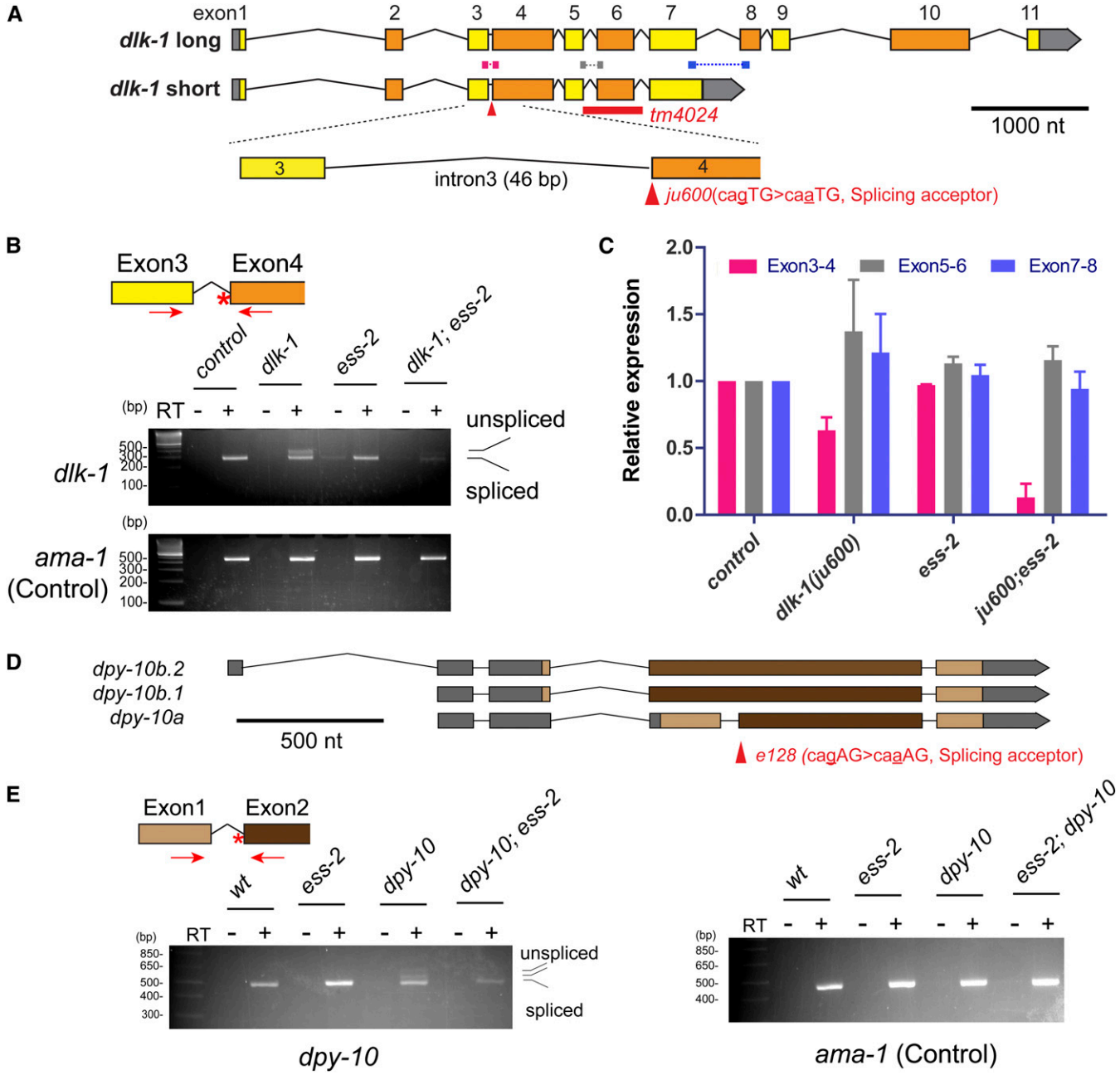

Figure 6 ESS-2 regulates mRNA splicing of cryptic transcripts. (A and D) Schematic diagrams of genomic loci of *dlk-1* and *dpy-10*. The *dlk-1* locus produces at least two isoforms, long (F33E2.2a) and short (F33E2.2c). *ju600* is a G-to-A substitution mutation located in the splice acceptor site of intron 3 as indicated by the arrowhead. Primers used for qRT-PCR in C are shown as bars and dashed lines between long and short isoforms. (B and E) Amounts of PCR products were analyzed by semiquantitative RT-PCR using *dlk-1* or *dpy-1* primers (red arrows). The positions of splice acceptor mutations in *dlk-1(ju600)* and *dpy-10(e128)* are shown by asterisks. The predicted sizes of spliced and unspliced fragments are indicated on the right side. *ama-1* encoding a large subunit of RNA polymerase II was used as a control. (C) Amounts of PCR products were analyzed by quantitative RT-PCR. The colors of bars match the amplified fragments indicated in A. All the strains in this experiment have *muIs32[Pmec-7-GFP]* and *rpm-1(ju44)* in the background. Error bar represents SEM; $n = 2$ biological replicates.

We selected genetic suppressor mutations based on behavioral improvement of the uncoordinated locomotion of *rpm-1* double mutants with *syd-1* or *syd-2*. We can draw the following conclusions from the analyses of a large number of genetic suppressor mutations. First, among 94 *rpm-1(lf)* suppressor alleles, we found nine alleles that were independent hits of the same nucleotide. Although the small number of genes and high hit rate per gene preclude the classical application of the Poisson distribution (Pollock and Larkin 2004), we reckon that this screen is likely saturated for the major components of the DLK-1 pathway. The design of our suppressor screen biases against genes whose loss of function results

in lethality or severe movement defects. Yet, we might expect to identify partial loss-of-function mutations in known essential genes as some suppressor mutations in the *dlk-1* cascade show rather weak activity. The absence of such mutations leads us to speculate that other genes may only have minor roles or act in parallel to modulate the six core components of the *dlk-1* cascade. Second, null mutants in the MLK-1/MEK-1/KGB-1 cascade are also homozygous viable; yet, our analysis indicates that this pathway does not have a major role in the context of synapse formation. The interaction between RPM-1 and this kinase pathway may be specific to other cellular contexts, such as axon regeneration (Nix *et al.* 2011). Third, most missense mutations in DLK-1/MKK-4/PMK-3 are in the kinase domains, highlighting the importance of the phosphorrelay in their action. The collection of functionally important mutations would provide additional information about how these proteins work when the three-dimensional structures of these proteins are available. Fourth, newly identified mutations in this study provide insights into how the components of the DLK-1 pathway function. For instance, the nonsense mutations in the C terminus of PMK-3 reside outside of the canonical kinase domain, implying its possible regulatory role. Furthermore, the missense mutation of CEBP-1 suggests an important role of the N terminus in its activity. As shown for other CEBP-1 orthologs, the N terminus of CEBP-1 may act as a transactivation domain (Pei and Shih 1991; Williams *et al.* 1995). Fifth, besides the core components of the DLK-1 kinase cascade, we identified a novel gene *supr-1* that antagonizes *rpm-1*. The lack of known motifs precludes us from drawing strong conclusions regarding the function of *supr-1*. Nonetheless, the observation that it is predominantly localized to the nucleus of neurons suggests that it may act through transcriptional or post-transcriptional modulation. Future studies, such as identifying its binding partners and/or targets will address such possibilities. Lastly, although our suppressor screen has an equal chance to identify mutations suppressing the behavioral defects of *syd-1* or *syd-2*, we found only a *sup-5* mutation as a suppressor of *syd-2*(Q397X) (this study) and a gain-of-function mutation in *syd-2* as a suppressor mutation of *syd-1* (Dai *et al.* 2006). This outcome contrasts to the large number of suppressors of *rpm-1*, and clearly reflects the nature of signaling contexts of these two pathways. RPM-1 negatively regulates a signal transduction cascade that largely acts in a linear manner, while SYD-1 and SYD-2 function in a concerted manner to promote the proper assembly or organization of an ensemble of proteins in presynaptic dense projections.

The DGCR14 protein ESS-2 is a splicing factor that ensures accurate splicing in a context-dependent manner

Our analysis of ESS-2 has provided the first functional evidence supporting a role of the conserved family of DGCR14 in mRNA splicing. The splicing machinery and process are highly conserved among metazoans (Rothman and Singson 2011). In *C. elegans* the 5′ splice site has the canonical metazoan consensus sequence AG/GURAGU (exon/intron), and most 3′ splice sites have a conserved sequence UUUUCAG/R (intron/exon). Despite the sequence conservation, a few studies show that mRNA splicing in *C. elegans* does not have stringent requirement for the CAG at the 3′ splice acceptor site, especially when the intron is short (Aroian *et al.* 1993; Zhang and Blumenthal 1996). A study demonstrated that an intron of 48 bp, which is a typical length in *C. elegans*, can be spliced out in the normal position despite mutations in the splice acceptor site, while longer introns (171 and 283 bp) are more dependent on canonical sequences at splice sites (Zhang and Blumenthal 1996). However, the mechanism of how accuracy of mRNA splicing is maintained for compromised or noncanonical splice sites still remains poorly understood. Our analysis of the splice acceptor mutation *dlk-1(ju600)* has added to our understanding of the mechanisms that ensure the fidelity of splice site selection. Intron 3 of *dlk-1* and intron 1 of *dpy-10* are 46 bp and 48 bp, respectively, and contain CAG at the 3′ splice site, which are mutated to CAA in *dlk-1(ju600)* and *dpy-10(e128)*. Our RT-PCR and qRT-PCR data indicate that these mutated introns can be properly spliced in the mutant animals, consistent with predictions from previous studies (Zhang and Blumenthal 1996). Although loss of function in *ess-2* does not alter this splicing step in wild type, it led to strongly impaired splicing in *dlk-1(ju600)* and *dpy-10(e128)*. Moreover, the dependency of *dlk-1(ju600)* on *ess-2(lf)* to suppress *rpm-1(lf)* provides functional evidence for the altered splicing. Together, these data support the role of ESS-2 in ensuring accurate mRNA splicing when the splice site is compromised and relies on noncanonical sequences.

mRNA splicing generally consists of two catalytic events, lariat intermediate formation in an intron and ligation of the two exons. In each step, splicing factors and snRNA components are dynamically exchanged and rearranged (Morton and Blumenthal 2011; Hegele *et al.* 2012). Among them the ribonucleoprotein complex that catalyzes the ligation step is called the C complex in which snRNAs and most proteins are conserved in *C. elegans* (Morton and Blumenthal 2011) (data not shown). The mammalian ES2/DGCR14 was found to coprecipitate with the C complex (Hegele *et al.* 2012), suggesting that ESS-2 may be functioning in the C complex in *C. elegans*. We found that both fully spliced and unspliced transcripts appeared to be reduced in *dlk-1(ju600)*; *ess-2(ju1117)* mutants, although the amount of transcripts was not changed. *ess-2(lf)* might cause intron 3 of *dlk-1(ju600)* transcripts to be stalled as a lariat structure, which might not be detected by RT-PCR and qRT-PCR. Further studies may address the precise effects of ESS-2 and its associated proteins in mRNA splicing. We observed similar effects on a *dpy-10* splice acceptor mutant, suggesting that ESS-2 function in splicing is widespread. We did not find any obvious phenotype nor splice deficiency in *ess-2* single mutant. This suggests that ESS-2 may play a redundant role with another component in C complex, or an accessory role in ensuring accurate splicing. As ESS-2 is a conserved protein from yeast to human, this mechanism ensuring accurate splicing may be conserved in higher organisms.

The fission yeast ortholog of ES2, Bis1, was found as an interacting protein to a stress-response nuclear envelope protein Ish1 (**i**nduced in **s**tationary p**h**ase 1) and plays a role in viability in the stationary phase (Taricani *et al.* 2002). Human ES2/DGCR14 is highly expressed in heart, brain, and skeletal muscle and is located in the common chromosome region on 22q11.2 deleted in patients with DiGeorge syndrome and velocardiofacial syndrome (Lindsay *et al.* 1996; Rizzu *et al.* 1996; Gong *et al.* 1997). Although these syndromes have been attributed to disruption of the T-box transcription factor, Tbx1, based on knockout studies in mice (Jerome and Papaioannou 2001; Lindsay *et al.* 2001; Merscher *et al.* 2001), it remains possible that deletion of ES2/DGCR14 may contribute to pathological progress in human patients through impaired splicing. Indeed, an analysis of point mutations associated with multiple human genetic diseases has estimated that up to 15% of all these mutations may result in mRNA splicing defects (Krawczak *et al.* 1992). Moreover, a recent study has suggested that promoter polymorphisms in the ES2/DGCR14 gene are associated with schizophrenia (Wang *et al.* 2006). Thus, examining *in vivo* targets of ESS-2 in the future will aid in better understanding the physiological roles of the ESS-2 family of proteins in higher organisms.

Acknowledgments

We gratefully acknowledge Mei Zhen and Xun Huang for their contribution in the early studies of synergistic interactions between *rpm-1* and *syd-1* or *syd-2* genes. We thank Gloriana Trujillo, Dong Yan, and Neset Ozel for noting the complex genetic traits of *dlk-1(ju600)*; past and present members of our laboratory for discussion and advice; and Andrew Chisholm for critical comments on the manuscript. We thank Shohei Mitani and the National Bioresearch Project (Tokyo Women's Medical University School of Medicine, Tokyo, Japan) and *C. elegans* knockout consortium for providing deletion alleles, Navin Pokala and Cornelia Bargmann for providing the code for the multiworm tracker prior to publication, and Seika Takayanagi-Kiya for her help in tracking analysis. Some of the strains were obtained from the *Caenorhabditis* Genetics Center, which is supported by grants from National Institutes of Health (NIH)–National Center for Research Resources. This work was supported by a grant from NIH to Y.J. (National Institute of Neurological Disorders and Stroke R01-035546). K.N. and A.G. are research associates and Y.J. is an investigator of the Howard Hughes Medical Institute.

Literature Cited

Ackley, B. D., and Y. Jin, 2004 Genetic analysis of synaptic target recognition and assembly. Trends Neurosci. 27: 540–547.

Aroian, R. V., A. D. Levy, M. Koga, Y. Ohshima, J. M. Kramer *et al.*, 1993 Splicing in Caenorhabditis elegans does not require an AG at the 3′ splice acceptor site. Mol. Cell. Biol. 13: 626–637.

Bigelow, H., M. Doitsidou, S. Sarin, and O. Hobert, 2009 MAQGene: software to facilitate C. elegans mutant genome sequence analysis. Nat. Methods 6: 549.

Bounoutas, A., J. Kratz, L. Emtage, C. Ma, K. C. Nguyen *et al.*, 2011 Microtubule depolymerization in Caenorhabditis elegans touch receptor neurons reduces gene expression through a p38 MAPK pathway. Proc. Natl. Acad. Sci. USA 108: 3982–3987.

Brenner, S., 1974 The genetics of *Caenorhabditis elegans*. Genetics 77: 71–94.

Ch'ng, Q., L. Williams, Y. S. Lie, M. Sym, J. Whangbo *et al.*, 2003 Identification of genes that regulate a left-right asymmetric neuronal migration in *Caenorhabditis elegans*. Genetics 164: 1355–1367.

Dai, Y., H. Taru, S. L. Deken, B. Grill, B. Ackley *et al.*, 2006 SYD-2 Liprin-[alpha] organizes presynaptic active zone formation through ELKS. Nat. Neurosci. 9: 1479–1487.

Delorenzi, M., and T. Speed, 2002 An HMM model for coiled-coil domains and a comparison with PSSM-based predictions. Bioinformatics 18: 617–625.

Dimitriadi, M., J. N. Sleigh, A. Walker, H. C. Chang, A. Sen *et al.*, 2010 Conserved genes act as modifiers of invertebrate SMN loss of function defects. PLoS Genet 6: e1001172.

Gong, W., B. S. Emanuel, N. Galili, D. H. Kim, B. Roe *et al.*, 1997 Structural and mutational analysis of a conserved gene (DGSI) from the minimal DiGeorge syndrome critical region. Hum. Mol. Genet. 6: 267–276.

Hall, D. H., and E. M. Hedgecock, 1991 Kinesin-related gene unc-104 is required for axonal transport of synaptic vesicles in C. elegans. Cell 65: 837–847.

Hallam, S. J., and Y. Jin, 1998 lin-14 regulates the timing of synaptic remodelling in Caenorhabditis elegans. Nature 395: 78–82.

Hallam, S. J., A. Goncharov, J. McEwen, R. Baran, and Y. Jin, 2002 SYD-1, a presynaptic protein with PDZ, C2 and rhoGAP-like domains, specifies axon identity in C. elegans. Nat. Neurosci. 5: 1137–1146.

Hegele, A., A. Kamburov, A. Grossmann, C. Sourlis, S. Wowro *et al.*, 2012 Dynamic protein-protein interaction wiring of the human spliceosome. Mol. Cell 45: 567–580.

Jerome, L. A., and V. E. Papaioannou, 2001 DiGeorge syndrome phenotype in mice mutant for the T-box gene, Tbx1. Nat. Genet. 27: 286–291.

Jin, Y., 2005 Synaptogenesis (December 23, 2005), *WormBook*, ed. The *C. elegans* Research Community, WormBook, doi/10.1895/wormbook.1.44.1, http://www.wormbook.org.

Jin, Y., and C. C. Garner, 2008 Molecular mechanisms of presynaptic differentiation. Annu. Rev. Cell Dev. Biol. 24: 237–262.

Krawczak, M., J. Reiss, and D. N. Cooper, 1992 The mutational spectrum of single base-pair substitutions in mRNA splice junctions of human genes: causes and consequences. Hum. Genet. 90: 41–54.

Liao, E. H., W. Hung, B. Abrams, and M. Zhen, 2004 An SCF-like ubiquitin ligase complex that controls presynaptic differentiation. Nature 430: 345–350.

Lindsay, E. A., P. Rizzu, R. Antonacci, V. Jurecic, J. Delmas-Mata *et al.*, 1996 A transcription map in the CATCH22 critical region: identification, mapping, and ordering of four novel transcripts expressed in heart. Genomics 32: 104–112.

Lindsay, E. A., E. L. Harvey, P. J. Scambler, and A. Baldini, 1998 ES2, a gene deleted in DiGeorge syndrome, encodes a nuclear protein and is expressed during early mouse development, where it shares an expression domain with a Goosecoid-like gene. Hum. Mol. Genet. 7: 629–635.

Lindsay, E. A., F. Vitelli, H. Su, M. Morishima, T. Huynh *et al.*, 2001 Tbx1 haploinsufficieny in the DiGeorge syndrome region causes aortic arch defects in mice. Nature 410: 97–101.

Maeder, C. I., and K. Shen, 2011 Genetic dissection of synaptic specificity. Curr. Opin. Neurobiol. 21: 93–99.

Mello, C. C., J. M. Kramer, D. Stinchcomb, and V. Ambros, 1991 Efficient gene transfer in C. elegans: extrachromosomal maintenance and integration of transforming sequences. EMBO J. 10: 3959–3970.

Merscher, S., B. Funke, J. A. Epstein, J. Heyer, A. Puech *et al.*, 2001 TBX1 is responsible for cardiovascular defects in velo-cardio-facial/DiGeorge syndrome. Cell 104: 619–629.

Morton, J. J., and T. Blumenthal, 2011 RNA processing in C. elegans. Methods Cell Biol. 106: 187–217.

Nakata, K., B. Abrams, B. Grill, A. Goncharov, X. Huang *et al.*, 2005 Regulation of a DLK-1 and p38 MAP kinase pathway by the ubiquitin ligase RPM-1 is required for presynaptic development. Cell 120: 407–420.

Nix, P., N. Hisamoto, K. Matsumoto, and M. Bastiani, 2011 Axon regeneration requires coordinate activation of p38 and JNK MAPK pathways. Proc. Natl. Acad. Sci. USA 108: 10738–10743.

Ou, C. Y., and K. Shen, 2010 Setting up presynaptic structures at specific positions. Curr. Opin. Neurobiol. 20: 489–493.

Patel, M. R., and K. Shen, 2009 RSY-1 is a local inhibitor of presynaptic assembly in C. elegans. Science 323: 1500–1503.

Pei, D. Q., and C. H. Shih, 1991 An "attenuator domain" is sandwiched by two distinct transactivation domains in the transcription factor C/EBP. Mol. Cell. Biol. 11: 1480–1487.

Pokala, N., Q. Liu, A. Gordus, and C. I. Bargmann, 2014 Inducible and titratable silencing of Caenorhabditis elegans neurons in vivo with histamine-gated chloride channels. Proc. Natl. Acad. Sci. USA 111: 2770–2775.

Pollock, D. D., and J. C. Larkin, 2004 Estimating the degree of saturation in mutant screens. Genetics 168: 489–502.

Rizzu, P., E. A. Lindsay, C. Taylor, H. O'Donnell, A. Levy *et al.*, 1996 Cloning and comparative mapping of a gene from the commonly deleted region of DiGeorge and Velocardiofacial syndromes conserved in C. elegans. Mamm. Genome 7: 639–643.

Rothman, J. H., and A. Singson, 2011 Caenorhabditis elegans: molecular genetics and development. Methods Cell Biol. 106: xv–xviii.

Sakaguchi, A., K. Matsumoto, and N. Hisamoto, 2004 Roles of MAP kinase cascades in Caenorhabditis elegans. J. Biochem. 136: 7–11.

Schaefer, A. M., G. D. Hadwiger, and M. L. Nonet, 2000 rpm-1, a conserved neuronal gene that regulates targeting and synaptogenesis in C. elegans. Neuron 26: 345–356.

Sudhof, T. C., 2012 The presynaptic active zone. Neuron 75: 11–25.

Taricani, L., M. L. Tejada, and P. G. Young, 2002 The fission yeast ES2 homologue, Bis1, interacts with the Ish1 stress-responsive nuclear envelope protein. J. Biol. Chem. 277: 10562–10572.

Trujillo, G., K. Nakata, D. Yan, I. N. Maruyama, and Y. Jin, 2010 A ubiquitin E2 variant protein acts in axon termination and synaptogenesis in *Caenorhabditis elegans*. Genetics 186: 135–145.

Wang, H., S. Duan, J. Du, X. Li, Y. Xu *et al.*, 2006 Transmission disequilibrium test provides evidence of association between promoter polymorphisms in 22q11 gene DGCR14 and schizophrenia. J. Neural Transm. 113: 1551–1561.

Waterston, R. H., and S. Brenner, 1978 A suppressor mutation in the nematode acting on specific alleles of many genes. Nature 275: 715–719.

White, J. G., E. Southgate, J. N. Thomson, and S. Brenner, 1986 The structure of the nervous system of the nematode Caenorhabditis elegans. Philos. Trans. R. Soc. Lond. B Biol. Sci. 314: 1–340.

Williams, S. C., M. Baer, A. J. Dillner, and P. F. Johnson, 1995 CRP2 (C/EBP beta) contains a bipartite regulatory domain that controls transcriptional activation, DNA binding and cell specificity. EMBO J. 14: 3170–3183.

Wills, N., R. F. Gesteland, J. Karn, L. Barnett, S. Bolten *et al.*, 1983 The genes sup-7 X and sup-5 III of C. elegans suppress amber nonsense mutations via altered transfer RNA. Cell 33: 575–583.

Yan, D., and Y. Jin, 2012 Regulation of DLK-1 kinase activity by calcium-mediated dissociation from an inhibitory isoform. Neuron 76: 534–548.

Yan, D., Z. Wu, A. D. Chisholm, and Y. Jin, 2009 The DLK-1 kinase promotes mRNA stability and local translation in C. elegans synapses and axon regeneration. Cell 138: 1005–1018.

Yan, D., K. Noma, and Y. Jin, 2011 Expanding views of presynaptic terminals: new findings from Caenorhabditis elegans. Curr. Opin. Neurobiol. 22: 431–437.

Zhang, H., and T. Blumenthal, 1996 Functional analysis of an intron 3′ splice site in Caenorhabditis elegans. RNA 2: 380–388.

Zhen, M., and Y. Jin, 1999 The liprin protein SYD-2 regulates the differentiation of presynaptic termini in C. elegans. Nature 401: 371–375.

Zhen, M., X. Huang, B. Bamber, and Y. Jin, 2000 Regulation of presynaptic terminal organization by C. elegans RPM-1, a putative guanine nucleotide exchanger with a RING-H2 finger domain. Neuron 26: 331–343.

Communicating editor: M. Sundaram

GENETICS

Supporting Information
http://www.genetics.org/lookup/suppl/doi:10.1534/genetics.114.167841/-/DC1

Systematic Analyses of *rpm-1* Suppressors Reveal Roles for ESS-2 in mRNA Splicing in *Caenorhabditis elegans*

Kentaro Noma, Alexandr Goncharov, and Yishi Jin

DOI: 10.1534/genetics.114.167841

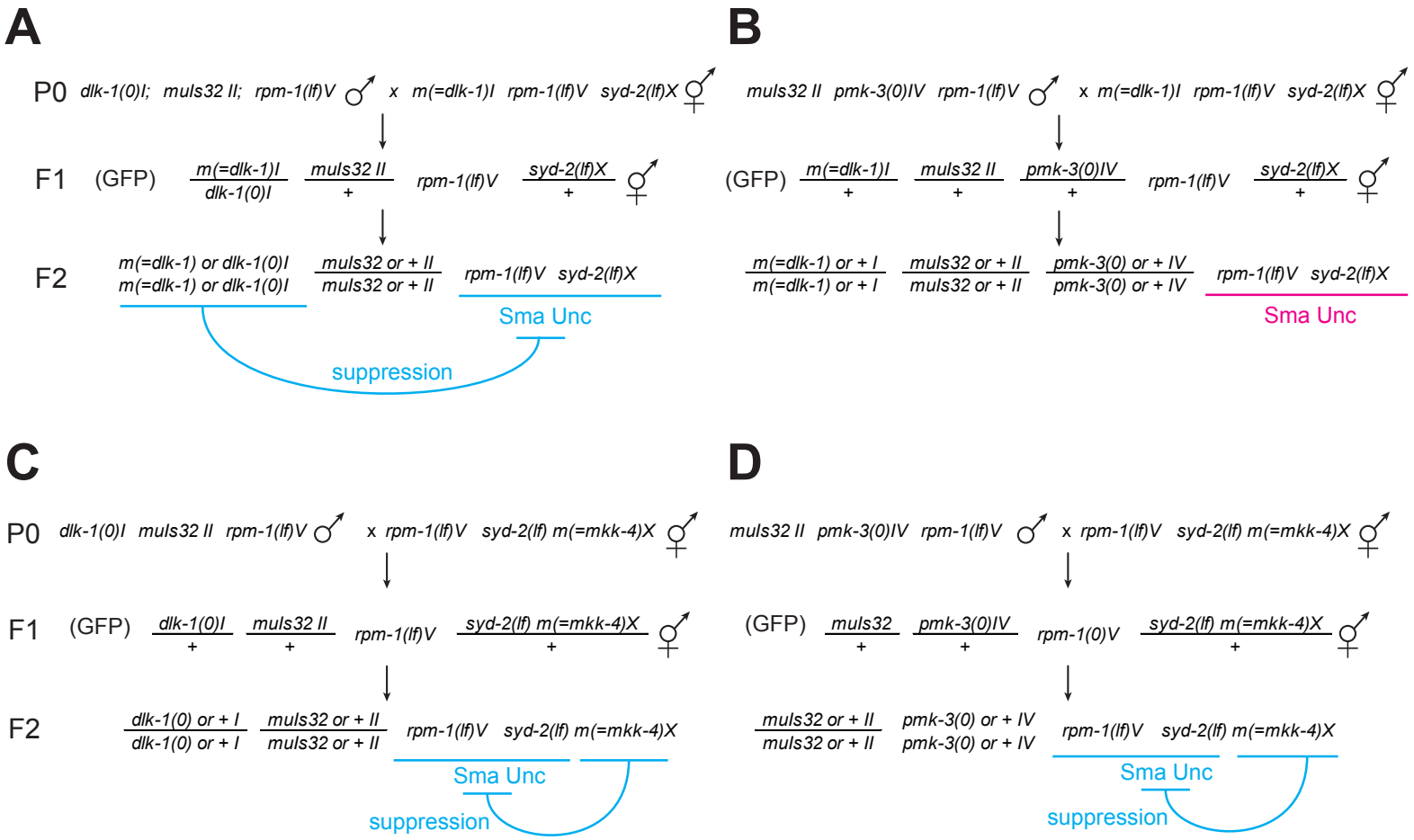

Figure S1 Complementation tests to *dlk-1* or *pmk-3.* Complementation tests were carried out to determine the identity of new suppressor mutations of *rpm-1* with respect to *dlk-1*, *pmk-3* and *mkk-4. rpm-1(ju44); syd-2(ju37);* suppressor mutant (shown as m) was crossed to *dlk-1(tm4024); muIs32; rpm-1(ju44)* (A and C) or *muIs32; pmk-3(ju485); rpm-1(ju44)* (B and D). *muIs32*-positive F1s are singled and self-fertilized. We examined whether any small and uncoordinated (Sma Unc) worms were present among the F2 progenies. Presence of Sma Unc worms due to *rpm-1(lf); syd-2(lf)* double-mutant background is an indication of complementation. *mkk-4* mutant appears to complement neither *dlk-1* nor *pmk-3* in this assay because it is tightly linked to *syd-2* (Figure 2C). (A) Complementation test with *dlk-1(0)* when a mutant is *dlk-1(lf)*. They do not complement each other. (B) Complementation test with *dlk-1(0)* when a mutant is *pmk-3(lf)*. They complement each other. (C and D) Complementation tests with *dlk-1(0)* and *pmk-3(0)* when a mutant is *mkk-4(lf)* in (C) and (D), respectively. Neither *dlk-1* nor *pmk-3* appears to complement *mkk-4.*

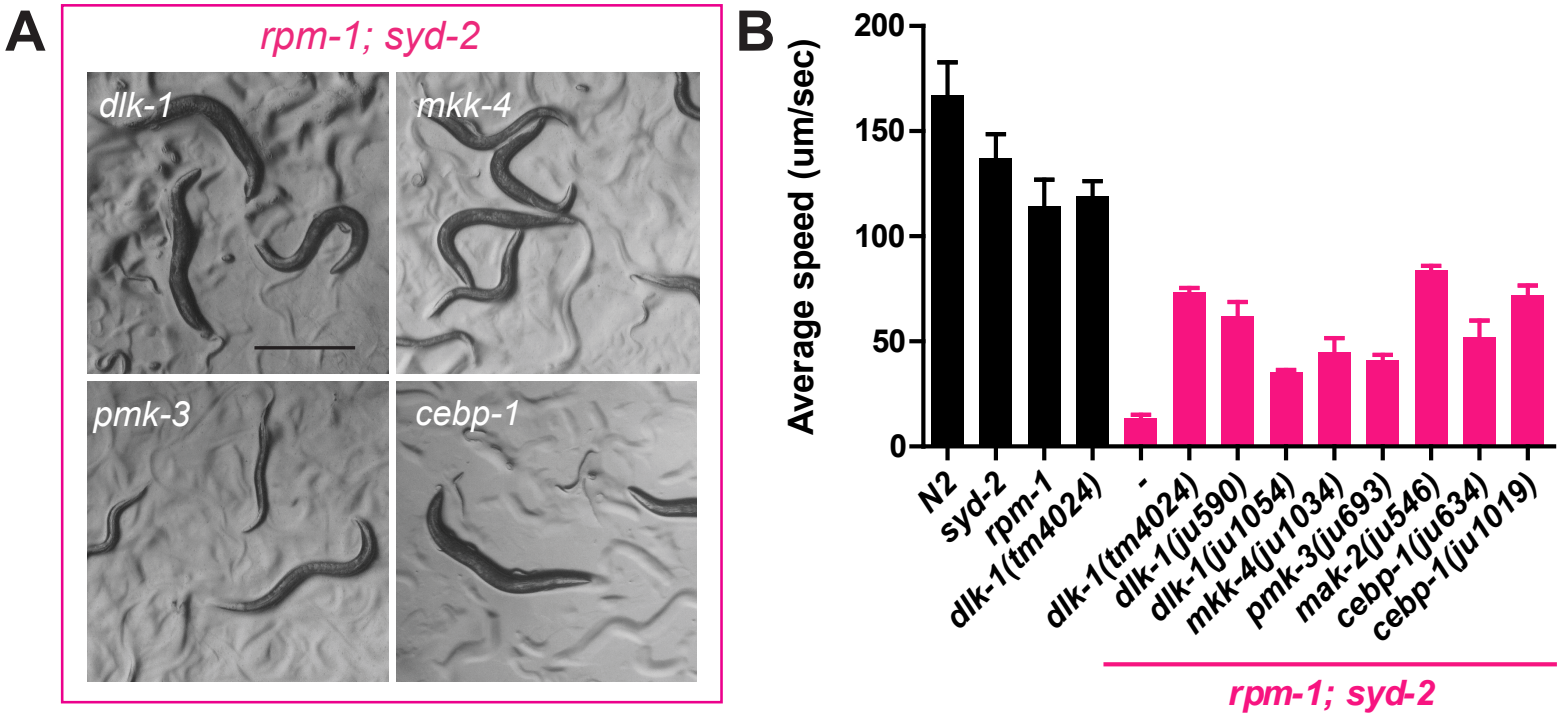

Figure S2 *rpm-1(lf); syd-2(lf)* body shape and movement phenotypes are suppressed by the mutations in the components of the DLK-1 pathway. (A) Bright-field images showing the body shapes of adult animals for the indicated genotypes. Scale bar: 500 μm. (B) The average velocities of the forward movement of the worms were analyzed as in Figure 1B. n=3 sessions, 5-10 worms in each session. Error bar indicates S.E.M.

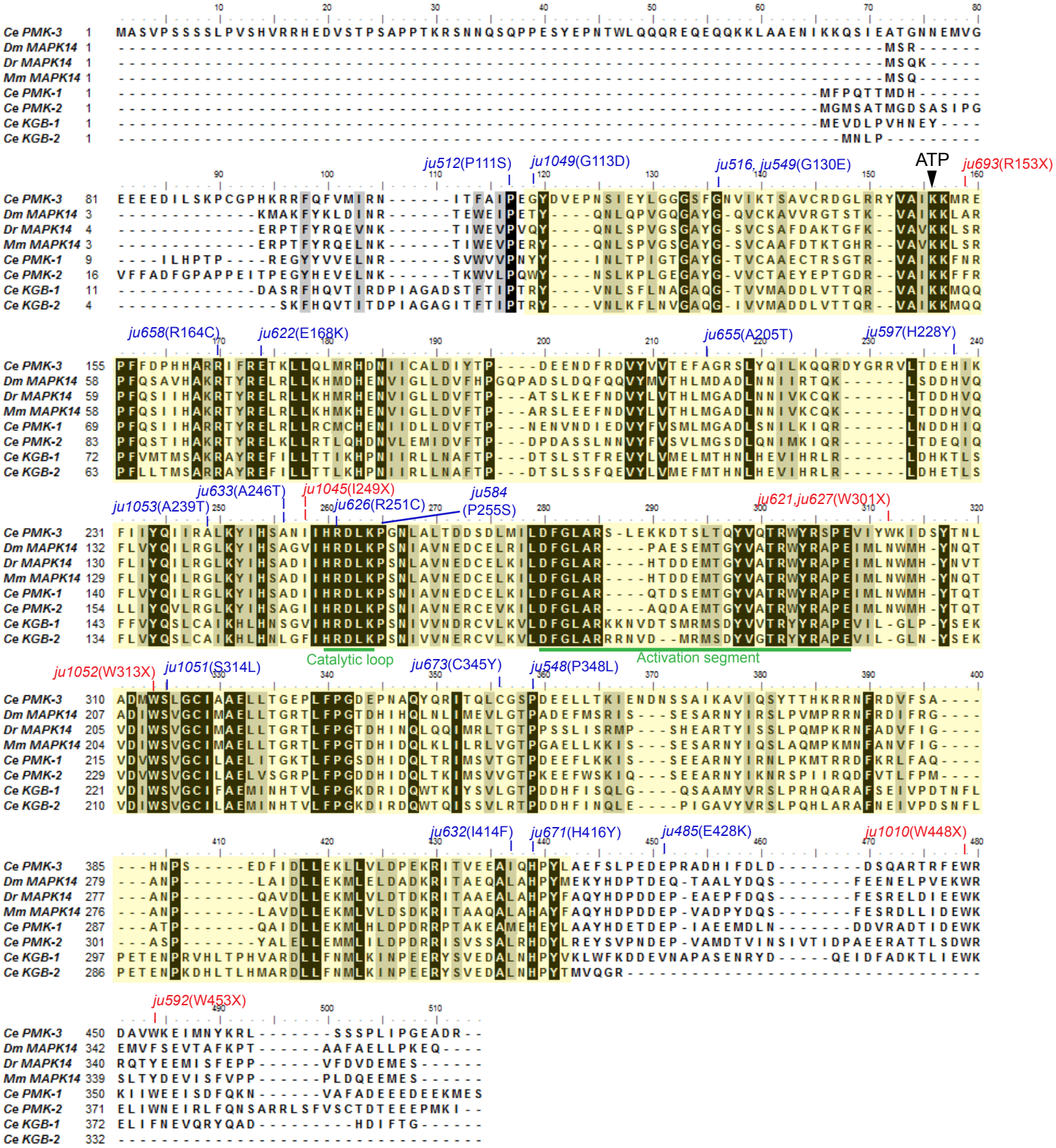

Figure S3 Alignment of PMK-3 orthologs and locations of *pmk-3(lf)* alleles identified as *rpm-1(lf)* suppressors. The alignment was obtained by the ClustalW multiple-alignment program. MAPK14/p38-α is shown as the PMK-3 ortholog in fly and vertebrates. The positions of nonsense (red) and missense (blue) mutations isolated as *rpm-1(lf)* suppressors in our study are shown above the sequences. Identical and similar residues are highlighted in black and gray, respectively. Kinase domain, based on UniProt, was shaded in yellow. The conserved ATP binding site is shown as a black arrowhead above the sequences. The conserved catalytic loop and activation segment are underlined in green. Species are *Ce: Caenorhabditis elegans; Dm: Drosophila melanogaster; Dr: Danio rerio; Mm: Mus musculus.* Accession numbers in UniProt are *Ce* PMK-3: O44514; *Dm* MAPK14: O61443; *Dr* MAPK14: Q9DGE2; *Mm* MAPK14: P47811; *Ce* PMK-1: Q17446; *Ce* PMK-2: Q8MXI4; *Ce* KGB-1: O44408; *Ce* KGB-2: H2KZI0.

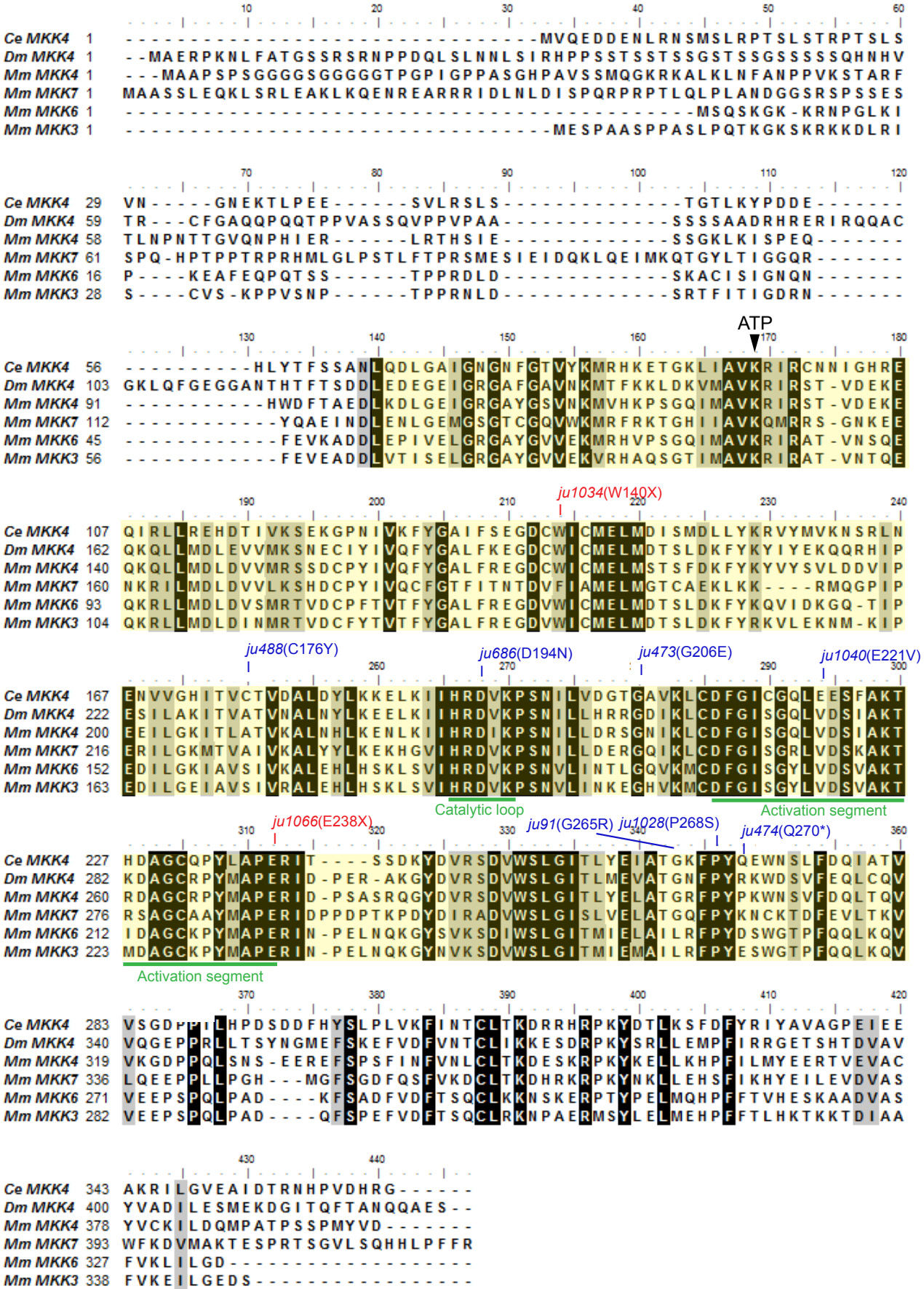

Figure S4 Alignment of MKK-4 homologs with *mkk-4(lf)* alleles suppressing *rpm-1(lf)*. The alignment was obtained by the ClustalW multiple-alignment program. The direct ortholog of C. elegans MKK-4 in mammals is MKK4 but mice have three other paralogs, MKK7, MKK3 and MKK6. The positions of nonsense (red) and missense (blue) mutations isolated as *rpm-1(lf)* suppressors in our study are shown above the sequences. Identical and similar residues are highlighted in black and gray, respectively. Kinase domain, based on UniProt, was shaded in yellow. The conserved ATP binding site is shown as a black arrowhead above the sequences. The conserved catalytic loop and activation segment are underlined in green. Species are *Ce: Caenorhabditis elegans; Dm: Drosophila melanogaster; Mm: Mus musculus.* Accession numbers in UniProt are *Ce* MKK-4: Q20347; *Dm* MKK4: O61444; *Mm* MKK4: P47809; *Mm* MKK7: Q8CE90-2; *Mm* MKK6: P70236; *Mm* MKK3: O09110.

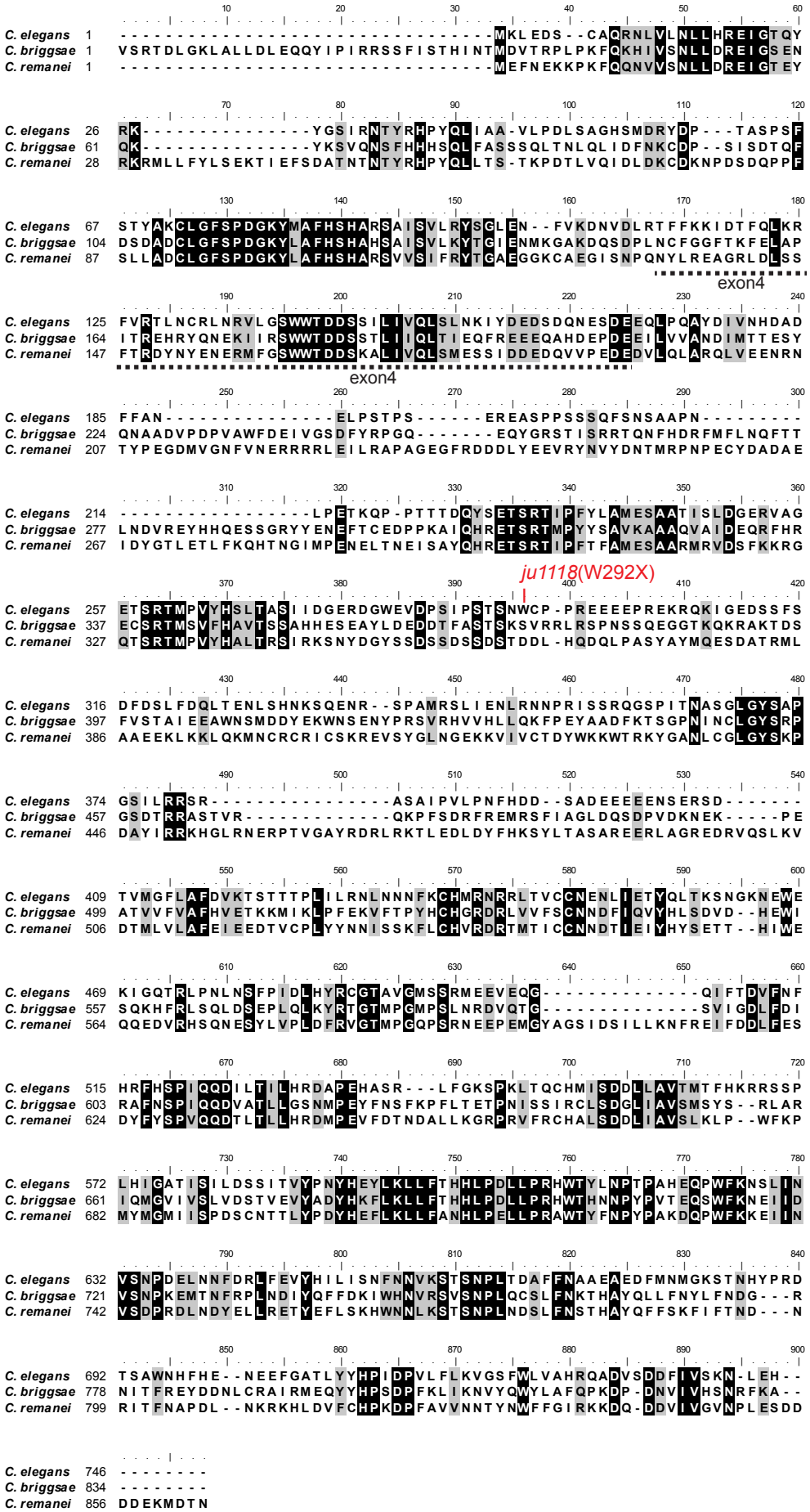

Figure S5 Alignment of SUPR-1 homologs. The alignment was obtained by the ClustalW multiple-alignment program. Identical and similar resides are highlighted in black and gray, respectively. The *rpm-1(lf)* suppressing allele *ju1118* is shown in red above the sequences. Accession number for *C. elegans* SUPR-1 in UniProt is Q95XT1. Accession numbers for *C. briggsae* and *C. remanei supr-1* in Wormbase are CBG04186 and CRE30057, respectively.

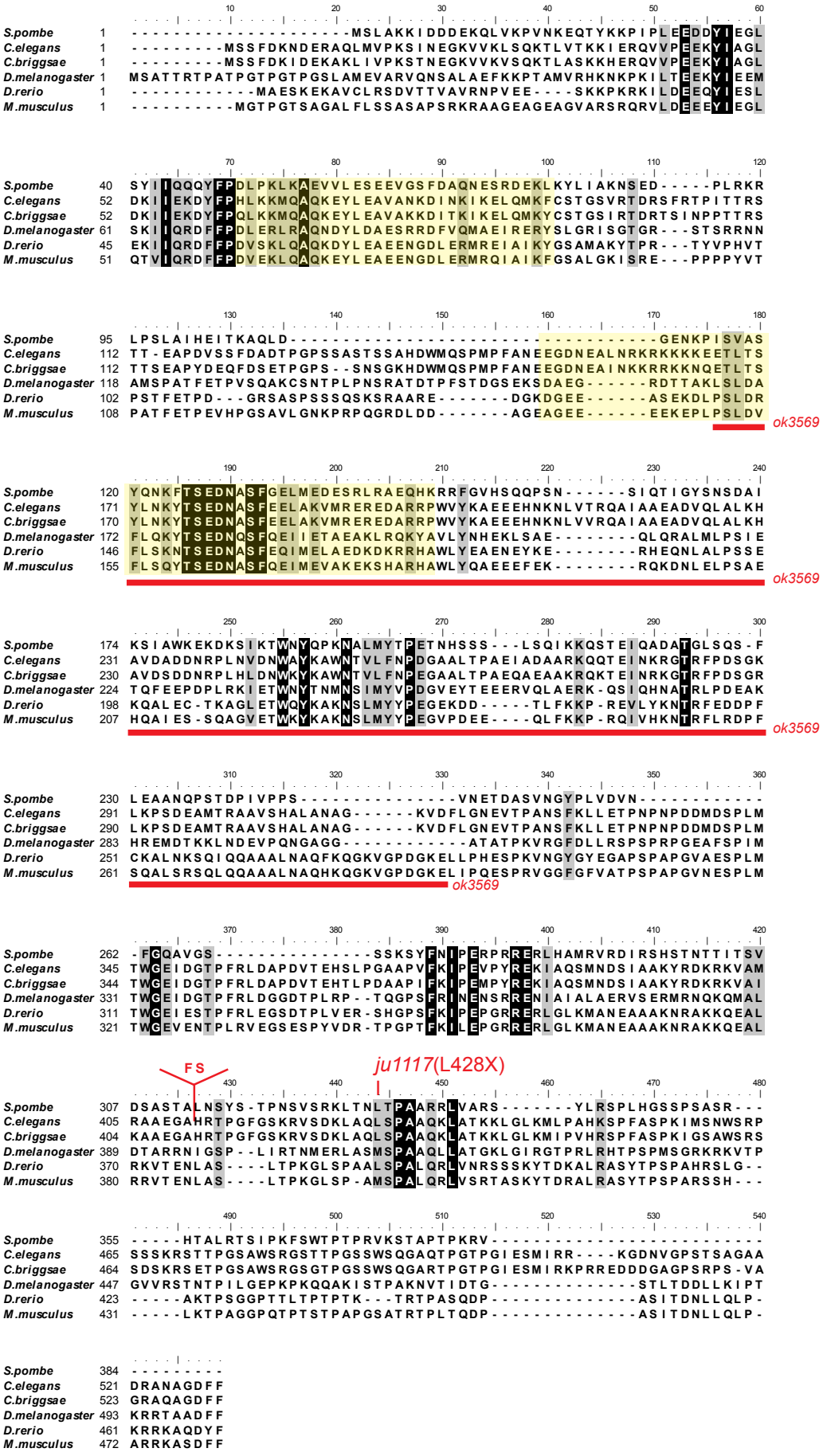

Figure S6 Alignment of ESS-2 homologs. The alignment was obtained by the ClustalW multiple-alignment program. Identical and similar resides are highlighted in black and gray, respectively. Deletion in *ok3569* mutant was confirmed by RT-PCR and is underlined in red. Two coiled-coil domains predicted by the MARCOIL program in *C. elegans* ESS-2 shaded in yellow (See Results). *C. elegans* ESS-2 b isoform has two additional residues, Phe and Ser, in the C-terminus compared to a isoform (shown as FS in red). The names of ESS-2 homologs and accession numbers in UniProt are the same as in Figure 5C.

Table S1 The list of *rpm-1(lf)* suppressor alleles

Gene	Allele	NT change	AA change	Domain	Gene	Allele	NT change	AA change	Domain
cebp-1	*ju1019*	G391T, C403T	A58S, Q62X		*mak-2*	*ju515**	G2049A	E53K	Kinase domain
cebp-1	*ju634*	G407C	R63P		*mak-2*	*ju567**	G2049A	E53K	Kinase domain
cebp-1	*ju602*	G938A	R240K	bZip domain	*mak-2*	*ju637*	C2316T	L142F	Kinase domain
cebp-1	*ju640*	C968T	S250L	bZip domain	*mak-2*	*ju546*	G2727A	Splice acceptor	Kinase domain
cebp-1	*ju659*	C970T	R251C	bZip domain	*mkk-4*	*ju1034*	G635A	W140X	Kinase domain
cebp-1	*ju695*	G979A	A254T	bZip domain	*mkk-4*	*ju488*	G742A	C176Y	Kinase domain
cebp-1	*ju1021*	C1057T	Q280X	bZip domain	*mkk-4*	*ju686*	G841A	D194N	Kinase domain
dlk-1	*ju600*	G2123A	Splice acceptor	Kinase domain	*mkk-4*	*ju473*	G878A	G206E	Kinase domain
dlk-1	*ju1046*	G2204A	G147E	Kinase domain	*mkk-4*	*ju1040*	A923T	E221V	Kinase domain
dlk-1	*ju687*	G2327A	G188E	Kinase domain	*mkk-4*	*ju1066*	G1225T	E238X	Kinase domain
dlk-1	*ju477*	G2364A	M200I	Kinase domain	*mkk-4*	*ju91*	G1350A	G265R	Kinase domain
dlk-1	*ju547*	G2442A	W226X	Kinase domain	*mkk-4*	*ju1028*	C1359T	P268S	Kinase domain
dlk-1	*ju624*	G2462A	G233E	Kinase domain	*mkk-4*	*ju474*	C1365T	Q270X	Kinase domain
dlk-1	*ju583*	T2465A	M234K	Kinase domain	*mkk-4*	*ju1026*	G1405A	Splice doner	Kinase domain
dlk-1	*ju692*	C2479T	Q239X	Kinase domain	*pmk-3*	*ju512*	C1841T	P111S	
dlk-1	*ju589**	G2500A	D246N	Kinase domain	*pmk-3*	*ju1049*	G1848A	G113D	
dlk-1	*ju660**	G2500A	D246N	Kinase domain	*pmk-3*	*ju516**	G1899A	G130E	kinase domain
dlk-1	*ju691*	G2554A	D264N	Kinase domain	*pmk-3*	*ju549**	G1899A	G130E	kinase domain
dlk-1	*ju551*	C2564T	T267M	Kinase domain	*pmk-3*	*ju693*	C2017T	R153X	kinase domain
dlk-1	*ju635*	G2601A	M279I	Kinase domain	*pmk-3*	*ju570*	G2341A	Splice acceptor	kinase domain
dlk-1	*ju599*	G2720A	M288I	Kinase domain	*pmk-3*	*ju658*	C2348T	R164C	kinase domain
dlk-1	*ju1031*	C2746T	Q296X	Kinase domain	*pmk-3*	*ju622*	G2360A	E168K	kinase domain
dlk-1	*ju648**	C2777T	S306L	Kinase domain	*pmk-3*	*ju655*	G2516A	A205T	kinase domain
dlk-1	*ju1037**	C2777T	S306L	Kinase domain	*pmk-3*	*ju597*	C2585T	H228Y	kinase domain
dlk-1	*ju588*	G2796A	W312X	Kinase domain	*pmk-3*	*ju1053*	G2618A	A239T	kinase domain
dlk-1	*ju625*	G2797A	E313K	Kinase domain	*pmk-3*	*ju633*	G2639A	A246T	kinase domain
dlk-1	*ju1035*	G2812A	E318K	Kinase domain	*pmk-3*	*ju1045*	T2822A	I249K	kinase domain
dlk-1	*ju630*	A2828T	N323I		*pmk-3*	*ju626*	G2828T	R251C	kinase domain
dlk-1	*ju619**	C3006T	P347S		*pmk-3*	*ju584*	C2839T	P255S	kinase domain
dlk-1	*ju1029**	C3006T	P347S		*pmk-3*	*ju621**	G2979A	W301X	kinase domain
dlk-1	*ju513*	C3033T	Q356X		*pmk-3*	*ju627**	G2979A	W301X	kinase domain
dlk-1	*ju586*	G3055A	R363H		*pmk-3*	*ju1052*	G3014A	W313X	kinase domain
dlk-1	*ju585**	C3060T	R365C		*pmk-3*	*ju1051*	C3017T	S314L	kinase domain
dlk-1	*ju623**	C3060T	R365C		*pmk-3*	*ju673*	G3110A	C345Y	kinase domain
dlk-1	*ju1032**	C3060T	R365C		*pmk-3*	*ju548*	C3119T	P348L	kinase domain
dlk-1	*ju590*	G3409A	Splice acceptor		*pmk-3*	*ju632*	A3316T	I414F	kinase domain
dlk-1	*ju591*	C3470T	L459P	Leucine zipper	*pmk-3*	*ju671*	G3322T	H416Y	kinase domain
dlk-1	*ju1044*	C3473T	Q460X	Leucine zipper	*pmk-3*	*ju485*	G3358A	E428K	
dlk-1	*ju598*	C3662T	R523X		*pmk-3*	*ju1010*	G3420A	W448X	
dlk-1	*ju596**	G4228A	W581X		*pmk-3*	*ju592*	G3516A	W453X	
dlk-1	*ju1039**	G4228A	W581X		*supr-1*	*ju1118*	G1933A	W292X	
dlk-1	*ju649*	G4296A	W604X		*uev-3*	*ju638*	G611A	Splice acceptor	
dlk-1	*ju694*	G4346A	Splice donor		*uev-3*	*ju593*	G1875A	Splice acceptor	UEV domain
dlk-1	*ju476*	After 4467	5 bp insertion		*uev-3*	*ju587*	G2058A	Splice acceptor	UEV domain
dlk-1	*ju653*	C5482T	Q700X		*uev-3*	*ju639*		26 bp deletion	UEV domain
dlk-1	*ju636*	C5830T	R816X						
dlk-1	*ju475**	C5929T	R849X						
dlk-1	*ju656**	C5929T	R849X						
dlk-1	*ju620*	G5993A	G870E	Activation peptide					

* The same mutations that were independently hit more than once from the different parental worms in our screen.

Table S2 The list of strains

Strain	Genotype
CZ1252	*rpm-1(ju44)*
CZ900	*syd-2(ju37)*
CZ1338	*juIs1; rpm-1(ju44); syd-2(ju37)*
CZ1339	*rpm-1(ju44); syd-2(ju37)*
CZ17301	*rpm-1(ju23); syd-2(ju37); juIs390[Prgef-1-RPM-1::GFP]*
CZ15454	*dlk-1(ju1054); juIs1; rpm-1(ju44); syd-2(ju37)*
CZ15434	*juIs1; rpm-1(ju44); mkk-4(ju1034) syd-2(ju37)*
CZ6506	*pmk-3(ju693) juIs1; rpm-1(ju44); syd-2(ju37)*
CZ15419	*juIs1; rpm-1(ju44); cebp-1(ju1019) syd-2(ju37)*
CZ1234	*rpm-1(ju23)*
CZ15956	*dlk-1(tm4024)*
CZ20842	*dlk-1(tm4024); juIs1; rpm-1(ju44); syd-2(ju37)*
CZ5180	*mak-2(ju546) juIs1; rpm-1(ju44); syd-2(ju37)*
CZ5320	*juIs1; rpm-1(ju44); cebp-1(ju634) syd-2(ju37)*
CZ333	*juIs1*
CZ4926	*juIs1; syd-2(ju37)*
CZ455	*juIs1; rpm-1(ju44)*
CZ8835	*muIs32*
CZ3073	*muIs32; rpm-1(ju44)*
CZ14005	*dlk-1(tm4024); muIs32; rpm-1(ju44)*
CZ17305	*uev-3(ju638); muIs32; rpm-1(ju44)*
CZ8456	*muIs32; mak-2(ok2394); rpm-1(ju44)*
CZ17322	*muIs32; rpm-1(ju44); cebp-1(tm2807)*
CZ7412	*muIs32; dpy-11(e224) rpm-1(ju44)*
CZ18388	*muIs32; ml-1(km19) dpy-11(e224) rpm-1(ju44)*
CZ17060	*muIs32; kgb-1(um3); rpm-1(ju44)*
CZ17072	*muIs32; kgb-1(um3) kgb-2(km16); rpm-1(ju44)*
CZ17589	*kgb-1(um3); rpm-1(ju44); syd-2(ju37)*
CZ17724	*supr-1(ju1118); muIs32; rpm-1(ju44)*
CZ17580	*supr-1(gk106345); muIs32; rpm-1(ju44)*
CZ17522	*supr-1(tm3467); muIs32; rpm-1(ju44)*
CZ18027	*supr-1(ju1118); muIs32; rpm-1(ju44); juEx5384[Pmec-4-SUPR-1(cDNA)]*
CZ18414	*supr-1(ju1118); muIs32; rpm-1(ju44); juEx5517[Pmec-4-GFP::SUPR-1(cDNA)]*
CZ18420	*juEx5517[Pmec-4-GFP::SUPR-1(cDNA)]*
CZ19707	*dlk-1(ju600); muIs32; rpm-1(ju44)*
CZ17520	*muIs32; ess-2(ju1117); rpm-1(ju44)*
CZ17518	*muIs32; ess-2(tm4246); rpm-1(ju44)*
CZ17585	*muIs32; ess-2(ok3569); rpm-1(ju44)*
CZ17519	*dlk-1(ju600); muIs32; ess-2(ju1117); rpm-1(ju44)*
CZ17517	*dlk-1(ju600); muIs32; ess-2(tm4246); rpm-1(ju44)*
CZ20928	*dlk-1(ju600); muIs32; ess-2(ok3569); rpm-1(ju44)*
CZ21083	*dlk-1(ju600); muIs32; ess-2(tm4246); rpm-1(ju44); juEx6352[Pess-2-ESS-2(gDNA)]*
CZ17593	*dlk-1(ju600); muIs32; ess-2(tm4246); rpm-1(ju44); juEx5241[Pmec-4-ESS-2(cDNA)]*
CZ19400	*dlk-1(ju600); muIs32; ess-2(tm4246); rpm-1(ju44); juEx5859[Pmec-4-ESS-2(cDNA)::GFP*
CZ19402	*dlk-1(ju600); muIs32; ess-2(tm4246); rpm-1(ju44); juEx5861Pmec-4-GFP::ESS-2(cDNA)]*
CZ21081	*dlk-1(ju600); muIs32; ess-2(tm4246); rpm-1(ju44); juEx6350[Pmec-4-ESS-2(ok3569)]*
CZ21082	*dlk-1(ju600); muIs32; ess-2(tm4246); rpm-1(ju44); juEx6351[Pmec-4-ESS-2(ju1117)]*
CZ19415	*juEx5859[Pmec-4-ESS-2(cDNA)::GFP]*
CZ18402	*ess-2(tm4246)*
CZ19531	*dpy-10(e128)*
CZ19532	*dpy-10(e128); ess-2(tm4246)*

**juIs1[Punc-25-SNB-1::GFP], muIs32[Pmec-7-GFP]*